On the Performance of Rate Splitting Multiple Access for ISAC in Device-to-Multi-Device IoT Communications

Sutanu Ghosh, *Member, IEEE,* Keshav Singh, *Member, IEEE*, Haejoon Jung, *Senior Member, IEEE*, Chih-Peng Li, *Fellow, IEEE*, and Trung Q. Duong, *Fellow, IEEE*

***Abstract*—In this paper, we analyze the performance of rate splitting multiple access (RSMA) technique for a multi-device communication system applying integrated sensing and communication (ISAC) to alleviate the problem of overlapping spectrum of radar signal and communication frequency bands. The system includes a cooperative access point (AP) which serves as a sensing node and a decode-and-forward (DF) relay to support the communication between a mobile device (MD) and multiple Internet-of-Things devices (IoDs). Assuming Nakagami fading channels, we provide an extensive analytical framework to evaluate the dual functionalities of the system considering various scenarios with different assumptions on blocklength, channel state information (CSI), and successive interference cancellation (SIC). In other words, we consider both infinite and finite blocklength transmissions under practical impairments including imperfect CSI and SIC. We investigate the outage probability (OP), and ergodic sum rate assuming infinite blocklength, while the block error rate (BLER), and goodput are analyzed in the finite blocklength regime. The closed-form and asymptotic expressions for the OP and BLER are presented. In addition, to evaluate the sensing performance, we derive the closed-form expressions of the false alarm and detection probabilities. Through the simulation results, we validate our analysis and delve into the impacts of various system parameters including transmit power, Nakagami shaping parameter, CSI error, SIC imperfection, the number of devices, and sensing threshold. Further, we observe that the proposed RSMA-based ISAC system provides higher ergodic sum rates compared to non-orthogonal multiple access (NOMA) both in the presence and absence of practical impairments.**

***Index Terms*—Rate splitting multiple access (RSMA), integrated sensing and communication (ISAC), cooperative communication, non-orthogonal multiple access (NOMA), outage probability (OP), Internet-of-Things (IoT).**

Sutanu Ghosh is with the Institute of Communications Engineering, National Sun Yat-sen University, Kaohsiung 80424, Taiwan. He is also with the Electronics and Communication Engineering, Institute of Engineering and Management, Kolkata, India (e-mail: sutanu99@gmail.com).

Keshav Singh and Chih-Peng Li are with the Institute of Communications Engineering, National Sun Yat-sen University, Kaohsiung 80424, Taiwan (e-mail: keshav.singh@mail.nsysu.edu.tw; cpli@faculty.nsysu.edu.tw).

Haejoon Jung is with the Department of Electronics and Information Convergence Engineering, Kyung Hee University, Yongin-si 17104, South Korea (e-mail:haejoonjung@khu.ac.kr).

Trung Q. Duong is with the Faculty of Engineering and Applied Science, Memorial University, St. John's, NL A1C 5S7, Canada, and with the School of Electronics, Electrical Engineering and Computer Science, Queen's University Belfast, BT7 1NN Belfast, U.K., and also with the Department of Electronic Engineering, Kyung Hee University, Yongin-si, Gyeonggi-do 17104, South Korea (e-mail: tduong@mun.ca).

The work of T. Q. Duong was supported in part by the Canada Excellence Research Chair (CERC) Program CERC-2022-00109.

Corresponding authors are Keshav Singh and Trung Q. Duong.

I. Introduction

The massive number of devices wirelessly connected to the Internet has made the Internet-of-Things (IoT) one of the leading paradigms for connecting the real world [1]. However, the fast growth of IoT networks creates various challenges, including spectrum congestion and throughput limitation. It is crucial to address all these challenging issues to ensure satisfactory quality of services. To eliminate spectrum congestion, sensing-communication coexistence (SCC) [2] and integrated sensing and communication (ISAC) [3] strategies are effective solutions. In SCC, both communication and sensing devices are operated autonomously, causing the typical problem of signal interference. In contrast to SCC, communication and sensing devices in ISAC are operated in a cooperative manner, which leads to an IoT paradigm shift [4].

ISAC is a radio emission technique, which is able to transmit data from the transmitter to the destination and also extract information from discrete echoes. Consequently, the combination of communication and sensing signals are tightly integrated. Based on the level of integration, there are several benefits such as improved hardware efficiency, spectrum efficiency, energy efficiency, and low latency. In general, ISAC can be realized through two different approaches - the integration of resources and the integration of various functionalities [5]. Recently, the attention is more focused on the latter in order to achieve high spectrum efficiency along with its cost-effectiveness. Radio frequency-based ISAC is a prominent technique to share spectrum and reuse hardware resources, and is anticipated to play a significant role in the next-generation wireless communication technologies [6]. Therefore, various research studies in waveform design, network design, and resource management have already been conducted following this approach. A recent study on energy-efficient adaptive channel sharing scheme in [7] shows the improvement of utilization efficiency of the spectrum resources using ISAC. Further, the benefit of ISAC-based systems to maximize the covert throughput is highlighted in [8].

The ISAC systems should be designed to guarantee end-to-end reliability while providing high enough data rate. For this reason, the elemental design issues of ISAC are studied in [15]. Further, the proposed ISAC-based network architecture in [16] can reduce the latency of sharing information among vehicles and enhance data rate while maintaining autonomous driving

TABLE I: A summary of a selected related work that considers ISAC.

Ref.	NOMA/RSMA	Perfect/Imperfect SIC, CSI	Hops	Type of fading	Metric
[9]	NOMA	PSIC, PCSI	1	Rayleigh	Secrecy rate, beam pattern
[10]	RSMA	PSIC, PCSI	1	-	Weighted sum rate, beam pattern value
[11]	NOMA	PSIC, PCSI	2	Rayleigh	Outage probability, ergodic capacity, probability of detection
[12]	NOMA	PSIC, PCSI	1	Rayleigh	Sensing efficiency, beam pattern, throughput
[13]	RSMA	PSIC, PCSI	1	Rayleigh	Root mean square error
[14]	NOMA	PSIC, PCSI	1	Nakagami	Outage probability, ergodic radar estimation information rate
Our work	RSMA	PSIC, ISIC, PCSI, ICSI	2	Nakagami	Outage probability, ergodic rate, block error rate, goodput, probability of false alarm, probability of detection

safety. However, it is difficult to support large information transmission at high data rate with limited spectrum allocation. For this reason, non-orthogonal transmission is employed in previous studies on ISAC. Accordingly, delay, throughput, and energy efficiency are improved using non-orthogonal multiple access (NOMA) compared to orthogonal multiple access (OMA). NOMA-based ISAC systems introduce non-orthogonality to the communication devices as well as non-orthogonality to the operation of communication and sensing [17]. The sensing performance in terms of sensing rate and the communication performance in terms of outage probability and communication rate are studied for NOMA-ISAC-based system in [18]. In addition, it can also provide better compatibility and more flexibility along with the ability to better utilize resources. However, its system performance is limited due to unwanted inter-communication-user-interference [9] and inter-functionality-interference [19]. Successive interference cancellation (SIC)-based approach is useful to tackle these concerns [20]. For instance, SIC is used in [21] to reduce the interference from dedicated sensing signals to the receivers which are connected to a base station. The objective of the work is to jointly optimize transmitted signals from the base station for communication and sensing to satisfy the desired beam pattern for sensing. An iterative channel estimation approach is applied for ISAC in [22] to achieve higher spectrum efficiency at lower bit error rates.

Cooperative communication techniques can also be exploited in ISAC to improve coverage and robustness through diversity gain in fading channels. In [23], the authors analyze the bit error rate performance for a downlink (DL) intelligent reflecting surface-assisted NOMA network where the intelligent reflecting surface acts as a relay node. In [24], NOMA with imperfect SIC (ISIC) is considered to analyze the outage probability (OP), ergodic capacity, energy efficiency performances of cooperative networks over α-μ fading channel. Based on the distance, a near user of DL NOMA-based network acts as a relay in [25] to support the communication between a base station and far user and the authors also solve a power allocation problem to minimize the OP. However, NOMA communication systems require complex receiver design while there is no generalized natural order for the channels of different users under NOMA-based system. In addition to that, the issue of the requirement of a large number of SIC operations is also involved with NOMA-based system.

To combat these issues, rate splitting multiple access (RSMA) is introduced in [26]. In RSMA, user information is split into two different parts: one for common information and the other for multiple private information. The common information is combined in a common signal and transmitted along with a private signal that includes separate information for each user. This is the major difference between RSMA and NOMA. In case of this multiple access technique, single-layer rate splitting does not require any user ordering, dynamic switching, or grouping at the transmit scheduler [27], as in NOMA, and single-layer of SIC at RSMA receivers can perform better compared to NOMA-based system. Hence, the superiority of RSMA over NOMA is well established in existing research for different network architectures [28]–[32]. Based on the utilization of the common stream of RSMA, it is established in [10] that there is no performance loss in the absence of radar signal. RSMA technique is also used for ISAC in [33] for dual-functional radar-communication satellite beamforming scheme to enable better communication-sensing trade-off and to achieve better target estimation performance. The effectiveness in simultaneously managing interference and achieving better trade-off between communications and sensing performance in low earth orbit-ISAC systems, RSMA is shown as an efficient technique in [34]. In Table I, a summary of the state-of-the-art NOMA and RSMA-based ISAC techniques are presented, which also clarify the distinctions of this work from the prior studies. As shown in the table, our work provides a more comprehensive performance analysis with various metrics under more general system assumptions.

Along with all the above discussions of the existing work, it should be noted that a half-duplex network needs two separate time intervals for two-way communications while a full-duplex network needs a single interval to do the same. However, the loop self interference (LSI) is an important problem in full-duplex networks, which is typically tackled by using natural isolation, time-domain elimination, and spatial suppression techniques [35]. Furthermore, the probability of detection and the probability of false alarm are also important performance metrics in ISAC to evaluate its ability to detect the target correctly [36], [37]. In [36], the authors assume that the amplitude estimation attains the Cramer-Rao lower bound, while in [37], the collocated and separated network architectures for both communication receiver and sensing target are considered in the case of a monostatic ISAC system.

A. Motivation and Contribution

It can be seen from the aforementioned discussion that ISAC-based cooperative communication can provide more resource utilization along with longer region of coverage area and better quality-of-service. In addition, it is also found that the joint framework of RSMA-based ISAC system along with multi-device communications can be a key ingredient for the next-generation wireless networks. Different from [11], RSMA-based ISAC system is adopted in this paper to upgrade the communication performance together with more effective utilization of various resources. Furthermore, unlike [11], this work presents cooperative communication between a mobile device and multiple IoT devices (IoDs) via an access point (AP) over more generalized Nakagami fading channel considering more practical impairments such as ISIC and imperfect channel state information (ICSI). In case of [11], authors analyze system performances for finite block length, while in our work, we analyze the performances of the system for both infinite and finite blocklength scenarios to consider ultra-reliable and low-latency communication (URLLC) with short packets. An extensive analytical framework is provided for the study of the reliability, rate, error, and target detection performances of the proposed architecture. The main contributions of this work are listed as follows.

- We provide an extensive performance analysis on the proposed RSMA-based ISAC system using various metrics under ISIC and ICSI.
- In the infinite blocklength regime, we analyze the OP, ergodic sum rate and present their closed-form expression for N IoDs associated downlink system. We also derive the asymptotic expressions of the OP at high signal-to-noise ratio (SNR) in both Nakagami and Rayleigh fading environments.
- For finite blocklength, we derive the block error rate (BLER), and goodput expressions. Further, because the exact expressions of the BLER is complex to compute, we adopt a linear approximation method for Q-function and use numerical integration to derive the closed-form expression of BLER.
- From the sensing perspective, we derive the expressions of the probability of detection and the probability of false alarm, which provides their exact trade-off for given sensing threshold limit and transmit power.
- The accuracy of analytical results is verified through the Monte-Carlo simulation. The numerical results are shown to highlight the impacts of the transmit power, ISIC and ICSI, Nakagami shaping parameter. In addition, the proposed RSMA-based ISAC system is more robust to ISIC and ICSI compared to NOMA.

Notation of various mathematical symbols used in the paper are listed with their meaning in Table II. The remaining portion of the paper is organized as follows. The system architecture of a downlink RSMA system is given in Section II. In Section III, we analyze the performance analyses for both infinite blocklength and finite blocklength and the asymptotic expressions are also given in Section III. The analysis of the probabilities of detection and false alarm is provided in Section IV. Simulation results are presented in Section V and finally the paper is concluded in Section VI.

TABLE II: Notation and definitions

Notation	Definitions
$f_u(.)$	Cumulative distribution function
$F_u(.)$	Probability density function
a_p, b_c,	Power allocation factors for common message
a_i, b_i,	Power allocation factors for private message
Υ_{RC}, Υ_{R,c_i}	SINRs for common message
Υ_{RP}, Υ_{R,p_i}	SINRs for private message
Υ_C^{th}, Υ_P^{th}	Threshold SNR of common and private message
$\mathcal{P}_{out}$	Outage probability
$\mathscr{P}(.)$	Probability of an event
$\Gamma(.,.)$, $\gamma(.,.)$	Upper, lower complete gamma function
$\Gamma(.)$	Gamma function
$D_U(.)$	Parabolic cylinder function
$\mathcal{R}_u$, ϵ_u	Instantaneous rate, achievable ergodic rate
$min(.,.)$	Minimum of two parameters
$Q(.)$, $Q(.,.)$	Q-function and Marcum Q-function
$E(.)$, $\mathcal{H}_u$	Expectation operator, Hypothesis
$\sqcup_r$, Λ	Instantaneous coding rate, channel dispersion
$\mathscr{R}_{ct}$, $\mathscr{R}_{pt}$	Target rate of common, private messages
φ_u, $\mathcal{G}_u$	BLER, goodput

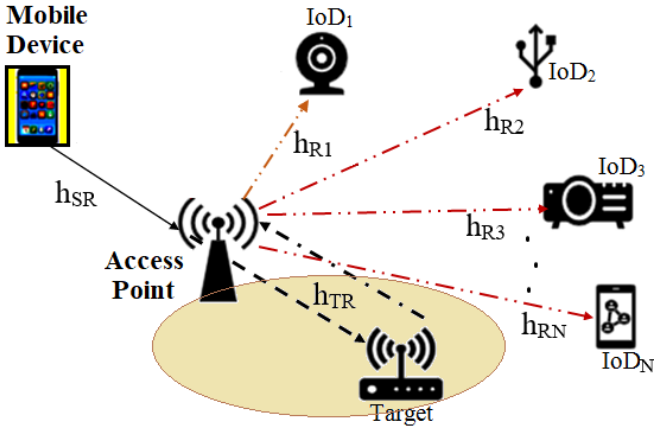

Fig. 1: Illustrative diagram of the system model using N IoDs and one target.

II. System Model

We consider a cooperative full-duplex DL ISAC network with a MD and N number of IoDs (IoD_1, IoD_2,...,IoD_N), as shown in Fig. 1. Further, Fig. 2 illustrates the timing diagram of the transmit and receive signals. The channels between the MD and IoDs are assumed to be very poor. Therefore, the MD takes help from a cooperative AP with the full-duplex capability to send its data successfully to IoDs. However, a target is present within the transmission zone of the AP and it is necessary for the AP to detect the signal from the target. The MD uses RSMA to transmit information via the AP towards IoDs located at different distances from the MD and the AP. Both the MD and the AP apply single-layer rate-splitting to avoid the user ordering at the transmitting end [38], [39]. The full-duplex decode-and-forward relaying ability is

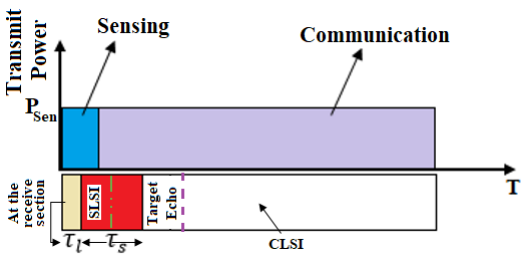

Fig. 2: Timing diagram of the transmit and receive signals.

considered at the AP to enhance the system performance in terms of communication. We assume that the MD and IoDs are equipped with a single antenna due to their space and power limitations.

The link coefficients between various channels MD $\rightarrow$ AP, AP $\rightarrow$ target $\sim$ target $\rightarrow$ AP and AP $\rightarrow$ IoD$_i$ are denoted by h_{SR}, $h_{RT} \sim h_{TR}$ and h_{Ri}, respectively. The link distances between various channels MD-AP, AP-target and AP-IoD$_i$ are denoted by d_{SR}, d_{TR} and d_{Ri}, respectively. It is assumed that all the channels follow Nakagami distribution to reflect general channel environments including Rayleigh fading. We also consider the effects of both imperfect SIC and ICSI for more realistic performance evaluation under practical impairments.

The transmitted signal from the MD during time t can be expressed as

$$X_s(t) = \sqrt{P_{MD}}\Big(\sqrt{a_p}s_p(t) + \sum_{i=1}^{N}\sqrt{a_i}s_i(t)\Big), \tag{1}$$

where P_{MD} is the transmission power of the MD. Also, a_p is the power allocation factor for the transmission of the common message indicated by $s_p(t)$, whilst a_i is the power allocation factor for the transmission of the private message indicated by $s_i(t)$. We note that $a_p + \sum_{i=1}^{N} a_i = 1$.

The AP transmits a separate signal $X_r(t)$ to the target in order to detect the target, which is expressed as

$$X_r(t) = \sqrt{P_{\text{Sen}}}x_R(t - \tau_R), \tag{2}$$

where τ_R indicates the duration of sensing signal and P_{Sen} is the transmitted power of the AP. Further, x_R is the transmitted symbol of AP. The AP can receive five signals: i) transmitted signal of the MD, ii) target echo reflected by the target, iii) communication LSI (CLSI) while transmitting the communication signal, iv) sensing LSI (SLSI) while transmitting sensing signal, v) additive white Gaussian noise (AWGN). Therefore, the received signal at the AP during any interval t can be expressed as

$$y_R(t) = \underbrace{\frac{(\hat{h}_{SR} + e_{SR})X_s(t)}{\sqrt{(d_{SR})^{\nu}}}}_{\text{BS signal}} + \underbrace{n_R(t)}_{\text{AWGN}} + \underbrace{\frac{(\hat{h}_{RR} + e_{RR})\sqrt{\lambda P_{\text{Sen}}}x_R(t - \tau_l - \tau_s)}{\sqrt{(d_{TR})^{\nu}}}}_{\text{Reflected signal from target}}$$
$$+ \frac{(\hat{h}_{LI} + e_{LI})\sqrt{\eta P_{\text{Sen}}}\Big(\overbrace{x_{CLI}(t - \tau_l)}^{\text{CLSI}} + \overbrace{x_{SLI}(t - \tau_l)}^{\text{SLSI}}\Big)}{\sqrt{(d_{Li})^{\nu}}}, \tag{3}$$

where $h_{SR} = \hat{h}_{SR} + e_{SR}$, $h_{RR} = \hat{h}_{RR} + e_{RR}$, $h_{Li} = \hat{h}_{Li} + e_{LI}$. Here, $\hat{h}_{SR}$, $\hat{h}_{RR}$, $\hat{h}_{Li}$ indicate the estimated channel gains, whereas e_{SR}, e_{RR}, e_{LI} are the channel estimation errors $e_{SR}, e_{RR}, e_{LI} \sim \mathcal{CN}(0, \sigma_R^2)$. Also, $\lambda \in [0, 1]$ indicates the target reflection factor and $\eta \in [0, 1]$ represents the LSI cancellation capability. Further, τ_l and τ_s are the time delays of the LSI and the target echo, respectively as shown in Fig. 2. h_{RR} is the cascaded channel of h_{RT} and h_{TR} to capture their composite effects. x_{CLI} and x_{SLI} are the CLSI and the SLSI at the AP by transmitting the communication and sensing signal, respectively, while ν indicates the path loss coefficient. As shown in Fig. 2, the received target signal interval $\tau_l + \tau_s$ is greater than transmitted signal interval τ_R.

The probability density functions (PDF) and cumulative distribution functions (CDFs) of the squared envelope of the channels h_{SR}, h_{LI}, h_{TR}, and h_{Ri} for $i \in \{1, 2, ..., N\}$ are respectively expressed as

$$f_{|h_{\varpi}|^2}(\delta) = \frac{n^n \delta^{n-1}}{\Gamma(n)} \exp(-n\delta), \tag{4}$$

$$F_{|h_{\varpi}|^2}(\delta) = \frac{1}{\Gamma(n)}\gamma(n, n\delta), \tag{5}$$

where $\delta \geq 0$, $\varpi \in \{SR, LI, TR, Ri\}$, and n is the shaping parameter. It is noted the PDF of CDF of the squared envelope $|h_{\varpi}|^2$ in (4) and (5) correspond to the gamma PDF and CDF, respectively, whereas the envelope of the channels (i.e., $|h_{\varpi}|$) follows the Nakagami distribution, as in [40, eq.(2.52)]. Further, the Nakagami distribution, which corresponds to the channel envelope $|h_{\varpi}|$, becomes equivalent to the Rayleigh distribution, when $n = 1$.

Over the cooperative link, the AP acts as a decode-and-forward (DF) relay and it decodes the common and private message of IoD$_i$ and treats the target echo, CLSI, and SLSI as interferences present with the communication signal. After proper detection of communicating signals transmitted from MD, AP forwards to IoDs [11]. Thus, the received signal at IoD$_i$ from the AP is expressed as (6), which is shown at the top of the next page. where $h_{Ri} = \hat{h}_{Ri} + e_{Ri}$ with $\hat{h}_{Ri}$ indicating the estimated channel gains. Also, e_{Ri} represents channel estimation error following a complex Gaussian distribution with zero-mean and variance of σ_D^2. Further, b_c and b_i are the power allocation factors of the common and private messages, respectively, where $b_c + \sum_{i=1}^{N} b_i = 1$. τ_C is decoding duration. For brevity, the function of variable t is not used in the subsequent portion of the paper.

Therefore, the received signal-to-interference plus noise ratio (SINR) of the common message of IoD$_i$ at the AP can be expressed as (7) at the top of the next page [41], where $\rho_{avg} = \frac{P_{MD}}{\sigma^2}$ and $\rho_R = \frac{P_{\text{Sen}}}{\sigma^2}$. After decoding of the common message, it applies SIC to eliminate the common message of IoD$_i$ from the received signal. To simplify the mathematical expressions, we define symbols as $A_1 = \frac{a_p \rho_{avg}}{d_{SR}^{\nu}}$,

$$y_{RD_i}(t) = \frac{(\hat{h}_{Ri}+e_{Ri})\sqrt{P_{\text{Sen}}}\Big(\sqrt{b_c}s_p(t-\tau_C)+\sqrt{b_i}s_i(t-\tau_C)\Big)}{\sqrt{(d_{Ri})^{\nu}}} + \sum_{j=1,i\neq j}^{N}\frac{(\hat{h}_{Ri}+e_{Ri})\sqrt{b_j P_{\text{Sen}}}s_j(t-\tau_C)}{\sqrt{(d_{Ri})^{\nu}}} + n_i(t), \quad (6)$$

$$\begin{aligned}\Upsilon_{RC} &= \frac{\frac{a_p\rho_{avg}|\hat{h}_{SR}|^2}{d_{SR}^{\nu}}}{1+\frac{\rho_{avg}|\hat{h}_{SR}|^2(1-a_p)}{d_{SR}^{\nu}}+\frac{\sigma_R^2\rho_{avg}}{d_{SR}^{\nu}}+\frac{2\eta\rho_R|\hat{h}_{LI}|^2}{d_{Li}^{\nu}}+\frac{2\eta\sigma_R^2\rho_R}{d_{Li}^{\nu}}+\frac{\lambda\rho_R|\hat{h}_{RR}|^2}{d_{TR}^{\nu}}+\frac{\lambda\sigma_R^2\rho_R}{d_{TR}^{\nu}}}\\ &= \frac{A_1|\hat{h}_{SR}|^2}{1+A_2|\hat{h}_{SR}|^2+A_3+B_1|\hat{h}_{LI}|^2+B_2+C_1|\hat{h}_{RR}|^2+C_2},\end{aligned} \quad (7)$$

$A_2=\frac{\rho_{avg}(1-a_p)}{d_{SR}^{\nu}}$, $A_3=\frac{\sigma_R^2\rho_{avg}}{d_{SR}^{\nu}}$, $B_1=\frac{2\eta\rho_R}{d_{Li}^{\nu}}$, $B_2=\frac{2\eta\sigma_R^2\rho_R}{d_{Li}^{\nu}}$, $C_1=\frac{\lambda\rho_R}{d_{TR}^{\nu}}$, and $C_2=\frac{\lambda\sigma_R^2\rho_R}{d_{TR}^{\nu}}$. Due to the interferences from both CLSI and SLSI, 2 is multiplied with $\frac{\eta\rho_R}{d_{Li}^{\nu}}$ and $\frac{\eta\sigma_R^2\rho_R}{d_{Li}^{\nu}}$ in B_1 and B_2. Therefore, the received SINR of the private message of IoD$_i$ at the AP can be expressed as (8) on the next page, where $A_4=\frac{\rho_{avg}}{d_{SR}^{\nu}}\sum_{j=1,i\neq j}^{N}a_j$, $A_5=\Theta_i A_1$, and $A_6=\frac{a_i\rho_{avg}}{d_{SR}^{\nu}}$. Further, Θ_i is the SIC imperfection factor at the AP, where $\Theta_i=0$ corresponds to the perfect SIC.

The SINR for the decoding of common message s_p at IoD$_i$ from the AP can be written as

$$\Upsilon_{R,c_i}=\frac{\frac{b_c\rho_R|\hat{h}_{Ri}|^2}{d_{Ri}^{\nu}}}{1+\frac{\rho_R|\hat{h}_{Ri}|^2(1-b_c)}{d_{Ri}^{\nu}}+\frac{\sigma_D^2\rho_R}{d_{Ri}^{\nu}}}=\frac{B_3|\hat{h}_{Ri}|^2}{1+B_4|\hat{h}_{Ri}|^2+C_3}, \quad (9)$$

where $B_3=\frac{b_c\rho_R}{d_{Ri}^{\nu}}$, $B_4=\frac{\rho_R(1-b_c)}{d_{Ri}^{\nu}}$, $C_3=\frac{\sigma_D^2\rho_R}{d_{Ri}^{\nu}}$, and σ^2 is the noise variance at IoD$_i$.

After decoding the common message, each of the devices applies SIC to eliminate the common message from the received signal and subsequently decodes its private message. Therefore, the SINR for decoding of the private message at IoD$_i$ can be written as

$$\begin{aligned}\Upsilon_{R,p_i} &= \frac{\frac{b_i\rho_R|\hat{h}_{Ri}|^2}{d_{Ri}^{\nu}}}{1+\frac{\rho_R|\hat{h}_{Ri}|^2}{d_{Ri}^{\nu}}\sum_{j=1,i\neq j}^{N}b_j+\frac{\sigma_D^2\rho_R}{d_{Ri}^{\nu}}+\frac{\Phi_i b_c\rho_R|\hat{h}_{Ri}|^2}{d_{Ri}^{\nu}}}\\ &= \frac{D_3|\hat{h}_{Ri}|^2}{1+B_6|\hat{h}_{Ri}|^2+C_3+C_4|\hat{h}_{Ri}|^2},\end{aligned} \quad (10)$$

where $B_6=\frac{\rho_R}{d_{Ri}^{\nu}}\sum_{j=1,i\neq j}^{N}b_j$, $C_4=\frac{\Phi_i b_c\rho_R}{d_{Ri}^{\nu}}$, and $D_3=\frac{b_i\rho_R}{d_{Ri}^{\nu}}$. In addition, Φ_i indicates the SIC imperfection factor at IoD$_i$, where $\Phi_i=0$ is equivalent to perfect SIC (PSIC).

III. Performance Analysis

In this section, we treat the performance analysis with infinite blocklength and finite blocklength in separate sub-sections. For the infinite blocklength case, in the first sub-section, we derive the outage probability (OP), ergodic sum rate, and asymptotic behavior of OP in the high SNR regime. Then, in the second sub-section, assuming finite blocklength, we analyze the block error rate (BLER), and goodput.

A. Infinite Blocklength Analysis

1) Outage Probability: We analyze the reliability of the proposed network in terms of OP, which is subject to the average SINR of the various links. The OP of IoD$_i$ can be defined as [41]

$$\begin{aligned}\mathcal{P}_{\text{out},i} &= 1-\underbrace{\mathscr{P}\big(\Upsilon_{RC}\geq\Upsilon_C^{th},\Upsilon_{RP}\geq\Upsilon_P^{th}\big)}_{\text{successful decoding of common and private message at AP}}\\ &\quad\times\underbrace{\mathscr{P}\big(\Upsilon_{R,c_i}\geq\Upsilon_C^{th},\Upsilon_{R,p_i}\geq\Upsilon_P^{th}\big)}_{\text{successful decoding of common and private message at IoD}_i}\\ &= 1-\Big(\mathscr{P}(\Upsilon_{RC}\geq\Upsilon_C^{th})\times\mathscr{P}(\Upsilon_{RP}\geq\Upsilon_P^{th})\\ &\quad\times\mathscr{P}(\Upsilon_{R,c_i}\geq\Upsilon_C^{th})\times\mathscr{P}(\Upsilon_{R,p_i}\geq\Upsilon_P^{th})\Big),\end{aligned} \quad (11)$$

where $\mathscr{P}(X)$ indicates the probability of event X, while Υ_C^{th} and Υ_P^{th} are the SNR thresholds of the common and private messages, respectively. For simplicity, suppose $|\hat{h}_{SR}|^2=x$, $|\hat{h}_{Ri}|^2=y$, $|\hat{h}_{LI}|^2=z$, and $|\hat{h}_{RR}|^2=v$. Then, based on [11, Eq. 67] and [42, Eq. 3.381.4, 3.462.1, 8.352.2], $\mathscr{P}(\Upsilon_{RC}\geq\Upsilon_C^{th})$ in (11) can be written as

$$\begin{aligned}&\mathscr{P}(\Upsilon_{RC}\geq\Upsilon_C^{th})=\mathscr{P}\Big((A_1-A_2\Upsilon_C^{th})x\\ &\qquad\geq\Upsilon_C^{th}(u_1+B_1z+C_1v)\Big)\\ &=\mathscr{P}\Big(x\geq\tfrac{u_1+B_1z+C_1v}{k_1}\Big)=\frac{2\sum_{p_a=0}^{n-1}\sum_{r=0}^{p_a}\sum_{t_k=0}^{p_a-r}\binom{p_a}{r}\binom{p_a-r}{t_k}}{p_a!(\Gamma n)^2\left(n+\frac{nB_1}{k_1}\right)^{n+r}k_1^{p_a}}\\ &(n+r-1)!B_1^r u_1^{p_a-r-t_k}C_1^{t_k}\exp\left(\frac{nk_1}{8C_1}-\frac{nu_1}{k_1}\right)n^{2n+p_a}\\ &\Gamma(n+2t_k+1)\left(2\frac{nC_1}{k_1}\right)^{-\frac{n+2t_k+1}{2}}D_{-n-2t_k-1}\left(\sqrt{\frac{nk_1}{2C_1}}\right),\end{aligned} \quad (12)$$

where $u_1=1+A_3+B_2+C_2$ and $k_1=\frac{(A_1-A_2\Upsilon_C^{th})}{\Upsilon_C^{th}}$, and $D_p(.)$ is parabolic cylider function. Similarly, $\mathscr{P}(\Upsilon_{RP}\geq\Upsilon_P^{th})$ can

$$\Upsilon_{RP} = \frac{\frac{a_i \rho_{avg} |\hat{h}_{SR}|^2}{d_{SR}^{\nu}}}{1 + \frac{\rho_{avg}|\hat{h}_{SR}|^2}{d_{SR}^{\nu}} \sum_{j=1, i\neq j}^{N} a_j + \frac{\sigma_R^2 \rho_{avg}}{d_{SR}^{\nu}} + \frac{\Theta_i a_p \rho_{avg} |\hat{h}_{SR}|^2}{d_{SR}^{\nu}} + \frac{2\eta\rho_R |\hat{h}_{LI}|^2}{d_{Li}^{\nu}} + \frac{2\eta\sigma_R^2\rho_R}{d_{Li}^{\nu}} + \frac{\lambda\rho_R|\hat{h}_{RR}|^2}{d_{TR}^{\nu}} + \frac{\lambda\sigma_R^2\rho_R}{d_{TR}^{\nu}}}$$
$$= \frac{A_6 |\hat{h}_{SR}|^2}{1 + A_4|\hat{h}_{SR}|^2 + A_3 + A_5|\hat{h}_{SR}|^2 + B_1|\hat{h}_{LI}|^2 + B_2 + C_1|\hat{h}_{RR}|^2 + C_2}, \tag{8}$$

be written as

$$\mathscr{P}(\Upsilon_{RP} \geq \Upsilon_P^{th}) = \mathscr{P}\bigg(x \geq \frac{\Upsilon_P^{th}(u_1 + B_1 z + C_1 v)}{(A_6 - A_4\Upsilon_P^{th} - A_5\Upsilon_P^{th})}\bigg)$$
$$= \mathscr{P}\Big(x \geq \tfrac{u_1 + B_1 z + C_1 v}{k_2}\Big) = \frac{2\sum_{p_a=0}^{n-1}\sum_{r=0}^{p_a}\sum_{t_k=0}^{p_a-r}\binom{p_a}{r}\binom{p_a-r}{t_k}}{p_a!(\Gamma n)^2\left(n+\frac{nB_1}{k_2}\right)^{n+r} k_2^{p_a}}$$
$$(n+r-1)! B_1^r u_1^{p_a-r-t_k} C_1^{t_k} \exp\left(\frac{nk_2}{8C_1} - \frac{nu_1}{k_2}\right) n^{2n+p_a}$$
$$\Gamma(n+2t_k+1)\left(2\frac{nC_1}{k_2}\right)^{-\frac{n+2t_k+1}{2}} D_{-n-2t_k-1}\left(\sqrt{\frac{nk_2}{2C_1}}\right), \tag{13}$$

where $k_2 = \frac{(A_6 - A_4\Upsilon_P^{th} - A_5\Upsilon_P^{th})}{\Upsilon_P^{th}}$. Moreover, we can simplify $\mathscr{P}(\Upsilon_{R,c_i} \geq \Upsilon_C^{th})$ and $\mathscr{P}(\Upsilon_{R,p_i} \geq \Upsilon_P^{th})$ as [42]

$$\mathscr{P}(\Upsilon_{R,c_i} \geq \Upsilon_C^{th}) = \frac{\Gamma(n, n\zeta_3)}{\Gamma(n)}, \tag{14}$$

$$\mathscr{P}(\Upsilon_{R,p_i} \geq \Upsilon_P^{th}) = \frac{\Gamma(n, n\zeta_4)}{\Gamma(n)}, \tag{15}$$

where $\zeta_3 = \frac{(1+C_3)\Upsilon_C^{th}}{B_3 - B_4\Upsilon_C^{th}}$ and $\zeta_4 = \frac{(1+C_3)\Upsilon_P^{th}}{D3 - B_6\Upsilon_P^{th} - C_4\Upsilon_P^{th}}$. If replacing (12)−(15) into (11), the exact OP at IoD$_i$ can be obtained in a closed form as (16) at the top of the next page.

Remark 1: It is observed that the exact OP in (16) *depends on the successful decoding of both common and private messages at both AP and IoD$_i$. Further, it must satisfy $\Upsilon_C^{th} < \frac{b_c}{1-b_c}$ and $\Upsilon_P^{th} < \frac{b_i}{\sum_{j=1,i\neq j}^{N} b_j + \Phi_i b_c}$. Otherwise, $\mathcal{P}_{out,i}$ boils down to 1. Also, we can observe that the overall outage performance is degraded (i.e., increases) with higher CSI error at both AP and IoDs, which is reflected in the term C_3 in ζ_3 and ζ_4. In addition, as the SIC imperfection factor Θ_i increases, the OP increases. Finally, it is also observed that, all the cumulative distribution functions of corresponding random variables are directly dependent on specific values of Nakagami shaping parameter, target reflection factor, loop self interference cancellation capability, common and private power allocation factors etc and accordingly, system performances vary.*

2) Asymptotic Outage Performance: To better understand the outage behavior with various system parameters, the closed-form expression in (16) is possible to simplify by considering the outage behavior at high SNR. At high SNR, $\exp(-\varsigma) = 1 - \varsigma$, $\Gamma(\mathcal{Z}, \varrho) \approx \Gamma(\mathcal{Z}) - \frac{\varrho^{\mathcal{Z}}}{\mathcal{Z}}$, $\varrho \ll 1$, $\mathcal{Z} > 0$ [42], and $D_{-v-\frac{1}{2}}(\mathcal{Y}) \approx (\mathcal{Y})^{-v-\frac{1}{2}}\left(1 - \frac{\mathcal{Y}^2}{4}\right)$ [43]. As a result, (16) can be approximated as (17) on the next page.

Lemma 1. *Consideration of special case with Rayleigh fading channels: Rayleigh fading channels corresponds to $n = 1$, the outage expression in* (16) *can be approximated further as follows [42, Eq. 3.322.2]*

$$\mathcal{P}_{out,i}^{\infty}|_{n=1} \approx \frac{\pi(1-\zeta_3-\zeta_4)\left(1 - \frac{u_1}{k_1} - \frac{u_1}{k_2} + \frac{k_1+k_2}{4C_1}\right)}{\frac{C_1^2}{k_1 k_2}\left(1 + \frac{B_1}{k_1} + \frac{B_1}{k_2} + \frac{B_1 B_2}{k_1 k_2}\right)}. \tag{18}$$

Remark 2: Based on (18)*, it is observed that the outage performance is degraded with increasing LSI. In fact, the performance is directly proportional to the complement of success, which is an increasing function of the shaping parameter n. Therefore, the worst-case scenario can be observed for $n = 1$, which corresponds to Rayleigh fading.*

3) Ergodic Sum Rate Analysis: The instantaneous rate at the AP for decoding common message is given by

$$\mathcal{R}_{RC} = \log_2(1 + \Upsilon_{RC}). \tag{19}$$

Using (19), the achievable ergodic rate for link between the MD and AP is computed as

$$\varepsilon_{RC} = \mathbb{E}[\mathcal{R}_{RC}], \tag{20}$$

where $\mathbb{E}[\cdot]$ denotes the statistical average. Further, the instantaneous rate at IoD$_i$ for decoding the common message is expressed as

$$\mathcal{R}_{R,c_i} = \log_2(1 + \Upsilon_{R,c_i}). \tag{21}$$

Accordingly, the achievable ergodic rate for the link between the AP and IoD$_i$ is given by

$$\varepsilon_{R,c_i} = \mathbb{E}[\mathcal{R}_{R,c_i}]. \tag{22}$$

Consequently, the overall ergodic sum rate for the common message is written as [44, Eq. 11]

$$\varepsilon_{Ci} = \Big(\min(\varepsilon_{RC}, \varepsilon_{R,c_i})\Big). \tag{23}$$

As in the common message case, the instantaneous rate at the AP for decoding the private message is

$$\mathcal{R}_{RP} = \log_2(1 + \Upsilon_{RP}). \tag{24}$$

From (24), the achievable ergodic rate for link between the MD and AP is computed as

$$\varepsilon_{RP} = \mathbb{E}[\mathcal{R}_{RP}]. \tag{25}$$

In the same manner, the instantaneous rate at IoD$_i$ for decoding the private message is written as

$$\mathcal{R}_{R,p_i} = \log_2(1 + \Upsilon_{R,p_i}), \tag{26}$$

$$\mathcal{P}_{\text{out},i} = 1 - \Bigg[\Bigg(\frac{2\sum_{p_a=0}^{n-1}\sum_{r=0}^{p_a}\sum_{t_k=0}^{p_a-r}\binom{p_a}{r}\binom{p_a-r}{t_k}(n+r-1)!B_1^r u_1^{p_a-r-t_k}C_1^{-\frac{n+1}{2}}n^{\frac{3}{2}n+p_a-t_k-\frac{1}{2}}\Gamma(n+2t_k+1)}{p_a!(\Gamma n)^2}\Bigg)^2$$
$$\times D_{-n-2t_k-1}\Bigg(\sqrt{\frac{nk_1}{2C_1}}\Bigg)\times D_{-n-2t_k-1}\Bigg(\sqrt{\frac{nk_2}{2C_1}}\Bigg)\times\frac{(k_1k_2)^{t_k+\frac{n+1}{2}-p_a}}{2^{t_k+\frac{n+1}{2}}}\times\frac{\exp\Bigg(\frac{nk_1}{8C_1}+\frac{nk_2}{8C_1}-\frac{nu_1}{k_1}-\frac{nu_1}{k_2}\Bigg)}{\Big[\big(n+\frac{nB_1}{k_1}\big)\big(n+\frac{nB_1}{k_2}\big)\Big]^{n+r}}$$
$$\times\frac{\Gamma(n,n\zeta_3)\times\Gamma(n,n\zeta_4)}{\big(\Gamma(n)\big)^2}\Bigg]. \quad (16)$$

$$\mathcal{P}^{\infty}_{\text{out},i} \approx 1 - \Bigg[\Bigg(\frac{2\sum_{p_a=0}^{n-1}\sum_{r=0}^{p_a}\sum_{t_k=0}^{p_a-r}\binom{p_a}{r}\binom{p_a-r}{t_k}C_1^{-\frac{n+1}{2}}}{p_a!(\Gamma n)^2}\Bigg)^2\times\big(B_1^r(n+r-1)!n^{\frac{3n-1}{2}+p_a-t_k}u_1^{p_a-r-t_k}\Gamma(n+2t_k+1)\big)^2$$
$$\times\Bigg(\frac{n}{2C_1}\sqrt{k_1k_2}\Bigg)^{-n-2t_k-1}\Bigg[1-\frac{n}{8C_1}\Big(k_1+k_2\Big)\Bigg]\times\frac{\Big(1-\frac{nu_1}{k_1}-\frac{nu_1}{k_2}+\frac{nk_1}{8C_1}+\frac{nk_2}{8C_1}\Big)(k_1k_2)^{t_k+\frac{n+1}{2}-p_a}}{\Big[\big(n+\frac{nB_1}{k_1}\big)\big(n+\frac{nB_1}{k_2}\big)\Big]^{n+r}2^{t_k+\frac{n+1}{2}}}$$
$$\times\frac{\big(\Gamma(n)-\frac{(n\zeta_3)^n}{n}\big)\big(\Gamma(n)-\frac{(n\zeta_4)^n}{n}\big)}{\big(\Gamma(n)\big)^2}\Bigg]. \quad (17)$$

where the achievable ergodic rate for link between the AP and IoD$_i$ is computed as

$$\varepsilon_{R,p_i} = \mathbb{E}[\mathcal{R}_{R,p_i}]. \quad (27)$$

Therefore, the overall ergodic sum rate for the private message is expressed as

$$\varepsilon_{Pi} = \Big(\min(\varepsilon_{RP},\varepsilon_{R,p_i})\Big). \quad (28)$$

According to the principle of RSMA, the overall sum rate can be expressed as

$$\varepsilon_s = \sum_{i\in N}\varepsilon_i = \sum_{i\in N}(\varepsilon_{C_i}+\varepsilon_{P_i}) = \varepsilon_{C_s}+\sum_{i\in N}\varepsilon_{P_i}, \quad (29)$$

where ε_{C_s} indicates the sum achievable ergodic rate for the common message of all users.

To derive the ergodic rate, we first obtain the CDF of Υ_{RC} as [42, Eq. 3.381.10, 8.354.1, 8.354.2, 8.356.3]

$$F_{\Upsilon_{RC}}(\Upsilon) = 1-\mathcal{P}(\Upsilon_{RC}\geq\Upsilon) = 1-\frac{\sum_{p_a=0}^{n-1}\sum_{r=0}^{p_a}\sum_{t_k=0}^{p_a-r}}{p_a!(\Gamma n)^2}$$
$$\sum_{t_j=0}^{\infty}\binom{p_a}{r}\binom{p_a-r}{t_k}(n+r-1)!B_1^r u_1^{p_a-r-t_k}C_1^{t_k-m_a}(-1)^{t_j}$$
$$\frac{n^{n+p_a+t_j-m_a-r}\Gamma(m_a)}{t_j!}\frac{\sum_{t_i=0}^{m_a+n+r-p_a}\binom{m_a+n+r-p_a}{t_i}(-1)^{t_i}}{\sum_{p_i=0}^{n+r}\binom{n+r}{p_i}(A_1)^{p_a-m_a-p_i}(B_1-A_2)^{p_i}}$$
$$\times\Big(\frac{A_2}{A_1}\Big)^{t_i}\Upsilon^{t_i+p_a-m_a-p_i}\exp\Big(-\frac{nu_1}{g(\Upsilon)}\Big), \quad (30)$$

where $m_a = \frac{n+2t_k+t_j+1}{2}$ and $g(\Upsilon) = \frac{(A_1-A_2\Upsilon)}{\Upsilon}$. Thus, the ergodic rate of the common message transfer from the MD to AP can be computed as

$$\varepsilon_{RC} = \mathbb{E}[\mathcal{R}_{RC}] = \frac{1}{\ln 2}\int_0^{\infty}\frac{1-F_{\Upsilon_{RC}}(\Upsilon)}{1+\Upsilon}d\Upsilon. \quad (31)$$

The exact expressions of ε_{RC} in (31) can be expressed as (32) [42, Eq. 3.381.4] as shown at the top of the next page. Similarly, the CDF of Υ_{RP} and it can be expressed as

$$F_{\Upsilon_{RP}}(\Upsilon) = 1-\mathcal{P}(\Upsilon_{RP}\geq\Upsilon) = 1-\frac{\sum_{p_a=0}^{n-1}\sum_{r=0}^{p_a}\sum_{t_k=0}^{p_a-r}}{p_a!(\Gamma n)^2}$$
$$\sum_{t_j=0}^{\infty}\binom{p_a}{r}\binom{p_a-r}{t_k}(n+r-1)!B_1^r u_1^{p_a-r-t_k}C_1^{t_k-m_a}(-1)^{t_j}$$
$$\frac{n^{n+p_a+t_j-m_a-r}\Gamma(m_a)}{t_j!}\frac{\sum_{t_i=0}^{m_a+n+r-p_a}\binom{m_a+n+r-p_a}{t_i}(-1)^{t_i}}{\sum_{p_i=0}^{n+r}\binom{n+r}{p_i}(A_6)^{p_a-m_a-p_i}(B_1-A_k)^{p_i}}$$
$$\times\Big(\frac{A_k}{A_6}\Big)^{t_i}\Upsilon^{t_i+p_a-m_a-p_i}\exp\Big(-\frac{nu_1}{h(\Upsilon)}\Big), \quad (33)$$

where $h(\Upsilon) = \frac{(A_6-A_4\Upsilon-A_5\Upsilon)}{\Upsilon}$ and $A_k = A_4+A_5$. As a result, the ergodic rate of the private message transfer from the MD to AP can be computed as

$$\varepsilon_{RP} = \mathbb{E}[\mathcal{R}_{RP}] = \frac{1}{\ln 2}\int_0^{\infty}\frac{1-F_{\Upsilon_{RP}}(\Upsilon)}{1+\Upsilon}d\Upsilon. \quad (34)$$

The exact mathematical expression of ε_{RP} in (34) can be obtained as (35) shown at the top of the next page. The ergodic

$$\varepsilon_{RC} = \frac{1}{\ln 2} \frac{\sum_{p_a=0}^{n-1} \sum_{r=0}^{p_a} \sum_{t_k=0}^{p_a-r} \sum_{t_j=0}^{\infty} \binom{p_a}{r} \binom{p_a-r}{t_k} (n+r-1)! B_1^r u_1^{p_a-r-t_k} C_1^{t_k-m_a}}{p_a!(\Gamma n)^2} \times \frac{(-1)^{t_j} n^{n+p_a+t_j-m_a-r}}{t_j!} \Gamma(m_a) \times \frac{\sum_{t_i=0}^{m_a+n+r-p_a} \binom{m_a+n+r-p_a}{t_i} (-1)^{t_i} \sum_{t_s=0}^{\infty} (-1)^{t_s}}{\sum_{p_i=0}^{n+r} \binom{n+r}{p_i} (B_1 - A_2)^{p_i}} \times \frac{A_1^{t_s+1} A_2^{t_i-p_k}}{\sum_{p_k=0}^{t_i+p_a-m_a-p_i+t_s+2} \binom{t_i+p_a-m_a-p_i+t_s+2}{p_k}} \times \frac{\Gamma(t_i+p_a+1-m_a-p_i+t_s-p_k)}{(nu_1)^{t_i+p_a+1-m_a-p_i+t_s-p_k}}. \quad (32)$$

$$\varepsilon_{RP} = \frac{1}{\ln 2} \frac{\sum_{p_a=0}^{n-1} \sum_{r=0}^{p_a} \sum_{t_k=0}^{p_a-r} \sum_{t_j=0}^{\infty} \binom{p_a}{r} \binom{p_a-r}{t_k} (n+r-1)! B_1^r u_1^{p_a-r-t_k} C_1^{t_k-m_a}}{p_a!(\Gamma n)^2} \times \frac{(-1)^{t_j} n^{n+p_a+t_j-m_a-r}}{t_j!} \Gamma(m_a) \times \frac{\sum_{t_i=0}^{m_a+n+r-p_a} \binom{m_a+n+r-p_a}{t_i} (-1)^{t_i} \sum_{t_s=0}^{\infty} (-1)^{t_s}}{\sum_{p_i=0}^{n+r} \binom{n+r}{p_i} (B_1 - A_k)^{p_i}} \times \frac{A_6^{t_s+1} A_k^{t_i-p_k}}{\sum_{p_k=0}^{t_i+p_a-m_a-p_i+t_s+2} \binom{t_i+p_a-m_a-p_i+t_s+2}{p_k}} \times \frac{\Gamma(t_i+p_a+1-m_a-p_i+t_s-p_k)}{(nu_1)^{t_i+p_a+1-m_a-p_i+t_s-p_k}}. \quad (35)$$

rate of common message transfer from the AP to IoD$_i$ can be computed as [42, Eq. 3.381.4]

$$\varepsilon_{R,c_i} = \mathbb{E}[\mathcal{R}_{R,c_i}] = \frac{1}{\ln 2} \int_0^{\infty} \frac{\Gamma\left(n, n\frac{(1+C_3)\Upsilon}{B_3 - B_4\Upsilon}\right)}{\Gamma(n)} \frac{d\Upsilon}{1+\Upsilon} = \frac{1}{\ln 2} \sum_{t_s=0}^{\infty} (-1)^{t_s} (B_3)^{t_s+1} \sum_{p_a=0}^{n-1} \frac{\left(n(1+C_3)\right)^{t_u-t_s-1}}{p_a! \sum_{t_u=0}^{t_s+2} \binom{t_s+2}{t_u} B_4^{t_u}} \Gamma(1+p_a+t_s-t_u). \quad (36)$$

Similarly, the ergodic rate of private message transfer from the AP to IoD$_i$ can be computed as

$$\varepsilon_{R,p_i} = \mathbb{E}[\mathcal{R}_{R,p_i}] = \frac{1}{\ln 2} \int_0^{\infty} \frac{\Gamma\left(n, n\frac{(1+C_3)\Upsilon}{D3 - B_6\Upsilon - C_4\Upsilon}\right)}{\Gamma(n)} \frac{d\Upsilon}{1+\Upsilon} = \frac{1}{\ln 2} \sum_{t_s=0}^{\infty} (-1)^{t_s} (D_3)^{t_s+1} \sum_{p_a=0}^{n-1} \frac{\left(n(1+C_3)\right)^{t_u-t_s-1}}{p_a! \sum_{t_u=0}^{t_s+2} \binom{t_s+2}{t_u} B_k^{t_u}} \Gamma(1+p_a+t_s-t_u), \quad (37)$$

where $B_k = B_6 + C_4$. Replacing (30)−(37), we can readily compute the overall ergodic rate for the common message ε_{C_i} in (23), the overall ergodic rate for the private message ε_{P_i} in (28), and, consequently, the overall sum rate ε_s in (29).

4) Asymptotic Ergodic Sum Rate Performance: To realize the nature of the ergodic sum rate, all the higher order terms are neglected for a special case and (32), (35), (36), (37) are simplified further at high SNR region. The simplified forms are as follows.

$$\varepsilon_{RC} \approx \frac{A_1}{\ln 2} \frac{n^{n-1}}{C_1^{\frac{n+1}{2}} u_1^{\frac{1-n}{2}}}, \quad (38)$$

$$\varepsilon_{RP} \approx \frac{A_6}{\ln 2} \frac{n^{n-1}}{C_1^{\frac{n+1}{2}} u_1^{\frac{1-n}{2}}}, \quad (39)$$

$$\varepsilon_{R,c_i} \approx \frac{B_3}{\ln 2} \frac{1}{n(1+C_3)}, \quad (40)$$

$$\varepsilon_{R,p_i} \approx \frac{D_3}{\ln 2} \frac{1}{n(1+C_3)}. \quad (41)$$

Remark 3: In the derived closed-form expressions in (32), (35), (36), (37) for any values of n and based on the above asymptotic expressions for Rayleigh fading, it can be observed that ergodic sum rate deteriorates with higher CSI errors. The ergodic rate for perfect channel state information (PCSI) and PSIC can be obtained as a special case with $\sigma_R = 0$ and $\Theta_i = 0$. Specifically, high SNR slopes are found as constants. It signifies that the scaling rates of the ergodic sum rates are not affected at high SNR region.

B. Finite Blocklength Analysis

1) Block Error Rate (BLER) Analysis: In this section, we analyze the reliability of the proposed network in terms of BLER. It is assumed that each transmission blocklength is r_k channel uses (CUs). The MD transmits ϑ bits during the transmission of packet $\sqcup_r$ and the instantaneous coding rate of the given system is $\sqcup_r = \vartheta / r_k$. The blocklength is assumed to be larger than 100. The average BLER for the common message can be computed as [45, Eq. 9]

$$\varphi_{\sqcap c} \approx \mathbb{E}\left\{ Q\left(\frac{\mathcal{R}_{\sqcap c} - \sqcup_r}{\sqrt{\Lambda_{\sqcap c}/r_k}} \right) \right\}, \quad (42)$$

where $\sqcap c \in \{(RC), (R, c_i)\}$ and the corresponding $\mathcal{R}_{\sqcap c}$ is given in (19) and (21), respectively. The symbol of channel dispersion $\Lambda_{\sqcap c} = \left(1 - 1/(1+\Upsilon_{\sqcap c})^2\right)(\log_2 e)^2$. Similarly, the average BLER for the private message is expressed as

$$\varphi_{\sqcap p} \approx \mathbb{E}\left\{ Q\left(\frac{\mathcal{R}_{\sqcap p} - \sqcup_r}{\sqrt{\Lambda_{\sqcap p}/r_k}} \right) \right\}, \quad (43)$$

where $\sqcap p \in \{(RP),(R,p_i)\}$ and the corresponding $\mathcal{R}_{\sqcap p}$ is given in (24) and (26), respectively. The symbol of channel dispersion $\Lambda_{\sqcap p} = \Big(1-1/(1+\Upsilon_{\sqcap p})^2\Big)(\log_2 e)^2$.

Moreover, the Q-function can be approximated in a linear form, which is expressed as $Q\left(\frac{\mathcal{R}_{\sqcap c}-\sqcup_r}{\sqrt{\Lambda_{\sqcap c}/r_k}}\right) \approx \phi(\sqcap c)$ [46, Eq. 14], [47, Eq. 54] with

$$\phi(\sqcap c) \;=\; \begin{cases} 1, & \Upsilon_{\sqcap c} \le \Xi_{\sqcap c}, \\ 0.5-\Delta_c\sqrt{r_k}(\Upsilon_{\sqcap c}-\chi_{\sqcap c}), & \Xi_{\sqcap c} \le \Upsilon_{\sqcap c} \le \mu_{\sqcap c}, \\ 0, & \Upsilon_{\sqcap c} \ge \mu_{\sqcap c}, \end{cases} \tag{44}$$

where $\Delta_c = \frac{1}{2\pi\sqrt{2^{2\sqcup_r}-1}}$, $\chi_{\sqcap c} = 2^{\sqcup_r}-1$, $\Xi_{\sqcap c} = \chi_{\sqcap c} - \frac{1}{2\pi\sqrt{r_k}}$, and $\mu_{\sqcap c} = \chi_{\sqcap c} + \frac{1}{2\pi\sqrt{r_k}}$.

By substituting (44) into (42), the average BLER for the common message can be written as

$$\varphi_{\sqcap c} \approx \int_0^{\infty} \phi_{\sqcap c}(X) f_{\Upsilon_{\sqcap c}}(X) dX, \tag{45}$$

where $f_{\Upsilon_{\sqcap c}}(X)$ is the PDF of $\Upsilon_{\sqcap c}$. We can apply integration by parts as

$$\varphi_{\sqcap c} \approx \Delta_c\sqrt{r_k} \int_{\Xi_{\sqcap c}}^{\mu_{\sqcap c}} F_{\Upsilon_{\sqcap c}}(X) dX. \tag{46}$$

Similarly, for the private message, we approximate the Q-function as $Q\left(\frac{\mathcal{R}_{\sqcap p}-\sqcup_r}{\sqrt{\Lambda_{\sqcap p}/r_k}}\right) \approx \phi(\sqcap p)$ with

$$\phi(\sqcap p) \;=\; \begin{cases} 1, & \Upsilon_{\sqcap p} \le \Xi_{\sqcap p}, \\ 0.5-\Delta_p\sqrt{r_k}(\Upsilon_{\sqcap p}-\chi_{\sqcap p}), & \Xi_{\sqcap p} \le \Upsilon_{\sqcap p} \le \mu_{\sqcap p}, \\ 0, & \Upsilon_{\sqcap p} \ge \mu_{\sqcap p}. \end{cases} \tag{47}$$

Using (47), $\varphi_{\sqcap p}$ can be written as

$$\varphi_{\sqcap p} \approx \Delta_p\sqrt{r_k} \int_{\Xi_{\sqcap p}}^{\mu_{\sqcap p}} F_{\Upsilon_{\sqcap p}}(Y) dY, \tag{48}$$

where $\Delta_p = \frac{1}{2\pi\sqrt{2^{2\sqcup_r}-1}}$, $\chi_{\sqcap p} = 2^{\sqcup_r}-1$, $\Xi_{\sqcap p} = \chi_{\sqcap p} - \frac{1}{2\pi\sqrt{r_k}}$, and $\mu_{\sqcap p} = \chi_{\sqcap p} + \frac{1}{2\pi\sqrt{r_k}}$.

Following [48], (46) and (48) are possible to compute using the Riemann integral identity $\int_a^b m(r_s)dr_s = (b-a)m\big((a+b)/2\big)$. Therefore, the BLERs in (46) and (48) can be simplified as

$$\varphi_{\sqcap c} \approx \Delta_c\sqrt{r_k}(\mu_{\sqcap c}-\Xi_{\sqcap c}) F_{\Upsilon_{\sqcap c}}\big((\Xi_{\sqcap c}+\mu_{\sqcap c})/2\big), \tag{49}$$

$$\varphi_{\sqcap p} \approx \Delta_p\sqrt{r_k}(\mu_{\sqcap p}-\Xi_{\sqcap p}) F_{\Upsilon_{\sqcap p}}\big((\Xi_{\sqcap p}+\mu_{\sqcap p})/2\big). \tag{50}$$

Now, the BLERs for the common messages (i.e., φ_{RC} and $\varphi_{R,c}$) and the BLERs for the private messages (i.e.,φ_{RP} and $\varphi_{R,p}$) can be expressed as

$$\varphi_{RC} \approx \Delta_c\sqrt{r_k}(\mu_{\sqcap c}-\Xi_{\sqcap c}) \Bigg[1 - \frac{\sum_{p_a=0}^{n-1}\sum_{r=0}^{p_a}\sum_{t_k=0}^{p_a-r}}{p_a!(\Gamma n)^2} \sum_{t_j=0}^{\infty} \binom{p_a}{r}\binom{p_a-r}{t_k}(n+r-1)!B_1^r u_1^{p_a-r-t_k} C_1^{t_k-m_a}(-1)^{t_j} \frac{n^{n+p_a+t_j-m_a-r}\Gamma(m_a)}{t_j!} \frac{\sum_{t_i=0}^{m_a+n+r-p_a}\binom{m_a+n+r-p_a}{t_i}\left(-\frac{A_2}{A_1}\right)^{t_i}}{\sum_{p_i=0}^{n+r}\binom{n+r}{p_i}(A_1)^{p_a-m_a-p_i}(B_1-A_2)^{p_i}} \big((\Xi_{\sqcap c}+\mu_{\sqcap c})/2\big)^{t_i+p_a-m_a-p_i} \exp\left(-\frac{nu_1}{g\big((\Xi_{\sqcap c}+\mu_{\sqcap c})/2\big)}\right)\Bigg], \tag{51}$$

$$\varphi_{R,c_i} \approx \Delta_c\sqrt{r_k}(\mu_{\sqcap c}-\Xi_{\sqcap c}) \times \left[\frac{\Gamma\left(n, n\frac{(1+C_3)\big((\Xi_{\sqcap c}+\mu_{\sqcap c})/2\big)}{B_3-B_4\big((\Xi_{\sqcap c}+\mu_{\sqcap c})/2\big)}\right)}{\Gamma(n)}\right], \tag{52}$$

$$\varphi_{RP} \approx \Delta_p\sqrt{r_k}(\mu_{\sqcap p}-\Xi_{\sqcap p}) \Bigg[1 - \frac{\sum_{p_a=0}^{n-1}\sum_{r=0}^{p_a}\sum_{t_k=0}^{p_a-r}}{p_a!(\Gamma n)^2} \sum_{t_j=0}^{\infty} \binom{p_a}{r}\binom{p_a-r}{t_k}(n+r-1)!B_1^r u_1^{p_a-r-t_k} C_1^{t_k-m_a}(-1)^{t_j} \frac{n^{n+p_a+t_j-m_a-r}\Gamma(m_a)}{t_j!} \frac{\sum_{t_i=0}^{m_a+n+r-p_a}\binom{m_a+n+r-p_a}{t_i}\left(-\frac{A_k}{A_6}\right)^{t_i}}{\sum_{p_i=0}^{n+r}\binom{n+r}{p_i}(A_6)^{p_a-m_a-p_i}(B_1-A_k)^{p_i}} \big((\Xi_{\sqcap p}+\mu_{\sqcap p})/2\big)^{t_i+p_a-m_a-p_i} \exp\left(-\frac{nu_1}{g\big((\Xi_{\sqcap p}+\mu_{\sqcap p})/2\big)}\right)\Bigg], \tag{53}$$

$$\varphi_{R,p_i} \approx \Delta_p\sqrt{r_k}(\mu_{\sqcap p}-\Xi_{\sqcap p}) \times \left[\frac{\Gamma\left(n, n\frac{(1+C_3)\big((\Xi_{\sqcap p}+\mu_{\sqcap p})/2\big)}{D3-(B_6+C_4)\big((\Xi_{\sqcap p}+\mu_{\sqcap p})/2\big)}\right)}{\Gamma(n)}\right], \tag{54}$$

respectively.

As a result, the total average BLER at the AP for the common and private messages can be expressed as

$$\varphi_{Ri} = (\varphi_{RC}+\varphi_{RP})/2. \tag{55}$$

On the other hand, the total average BLER at any of the all IoDs for common message and private message can be expressed as

$$\varphi_{Di} = (\varphi_{R,c_i}+\varphi_{R,p_i})/2. \tag{56}$$

Therefore, the overall average BLER of the proposed network for all IoDs can be expressed as [49]

$$\varphi_N = \frac{1}{N}\sum_{i=1}^{N}\Big(\varphi_{Ri} + \big(1-\varphi_{Ri}\big)\times\varphi_{Di}\Big). \tag{57}$$

2) Asymptotic Analysis of BLER: The expressions in (51)−(54) are possible to simplify further by considering in high SNR regime.

Lemma 2. *At high SNR,* $\exp(-\varsigma) = 1-\varsigma$, $\Gamma(\mathcal{Z},\varrho) \approx \Gamma(\mathcal{Z}) - \frac{\varrho^{\mathcal{Z}}}{\mathcal{Z}}$, $\varrho \ll 1$, $\mathcal{Z} > 0$, *and higher order terms are neglected for a special case. Hence* (51)−(54) *can be approximated as*

$$\varphi_{RC}^{\infty} \approx \Delta_c \sqrt{r_k}(\mu_{\sqcap c} - \Xi_{\sqcap c}) \Bigg[1 - \frac{n^{\frac{n-1}{2}}}{\left(\frac{C_1}{A_1}\right)^{\frac{n+1}{2}}} \times \left((\Xi_{\sqcap c} + \mu_{\sqcap c})/2\right)^{-\frac{n+1}{2}} \left(1 - \frac{nu_1}{g\left((\Xi_{\sqcap c} + \mu_{\sqcap c})/2\right)}\right)\Bigg], \quad (58)$$

$$\varphi_{R,c_i}^{\infty} \approx \Delta_c \sqrt{r_k}(\mu_{\sqcap c} - \Xi_{\sqcap c}) \times \left[1 - \frac{\left(n\frac{(1+C_3)\left((\Xi_{\sqcap c}+\mu_{\sqcap c})/2\right)}{B_3 - B_4\left((\Xi_{\sqcap c}+\mu_{\sqcap c})/2\right)}\right)^n}{n!}\right], \quad (59)$$

$$\varphi_{RP}^{\infty} \approx \Delta_p \sqrt{r_k}(\mu_{\sqcap p} - \Xi_{\sqcap p}) \Bigg[1 - \frac{n^{\frac{n-1}{2}}}{\left(\frac{C_1}{A_6}\right)^{\frac{n+1}{2}}} \times \left((\Xi_{\sqcap p} + \mu_{\sqcap p})/2\right)^{-\frac{n+1}{2}} \left(1 - \frac{nu_1}{g\left((\Xi_{\sqcap p} + \mu_{\sqcap p})/2\right)}\right)\Bigg], \quad (60)$$

$$\varphi_{R,p_i}^{\infty} \approx \Delta_p \sqrt{r_k}(\mu_{\sqcap p} - \Xi_{\sqcap p}) \times \left[1 - \frac{\left(n\frac{(1+C_3)\left((\Xi_{\sqcap p}+\mu_{\sqcap p})/2\right)}{D3 - (B_6+C_4)\left((\Xi_{\sqcap p}+\mu_{\sqcap p})/2\right)}\right)^n}{n!}\right], \quad (61)$$

respectively.

Remark 4: In the derived expressions, we observe that BLER performances significantly degrade with higher CSI errors. Similar to ergodic sum rate, average BLER for PCSI and PSIC can be computed as a special case with $\sigma_R = 0$ *and* $\Theta_i = 0$. *Furthermore, based on* (58)−(61)*, we can conclude that the BLER at each IoD and overall average BLER in* (57) *improves (decreases) by adjusting the Nakagami factor* n. *At high SNR, the errors associated with the received transport block at IoDs are very less, which indicates low BLER. It may be also noted that the improvement of BLER with* n *is not significant at very high SNR region.*

3) Goodput Analysis: The goodput is another important performance metric to quantify the delivery of useful data over the network per unit of allocated time. The goodput at the AP can be written as

$$\mathcal{G}_{Ri} = \left(1 - \frac{r_{lk,i}}{r_k}\right)\mathscr{R}_{ct}(1-\varphi_{RC}) + \left(1 - \frac{r_{lk,i}}{r_k}\right)\mathscr{R}_{pt}(1-\varphi_{RP}), \quad (62)$$

where $r_{lk,i} = r_k - \vartheta$. $\mathscr{R}_{ct}$ and $\mathscr{R}_{pt}$ are the target rates of common and private messages, respectively. Similarly, the goodput at IoD_i can be written as

$$\mathcal{G}_{Di} = \left(1 - \frac{r_{lk,i}}{r_k}\right)\mathscr{R}_{ct}(1-\varphi_{R,c_i}) + \left(1 - \frac{r_{lk,i}}{r_k}\right)\mathscr{R}_{pt}(1-\varphi_{R,p_i}). \quad (63)$$

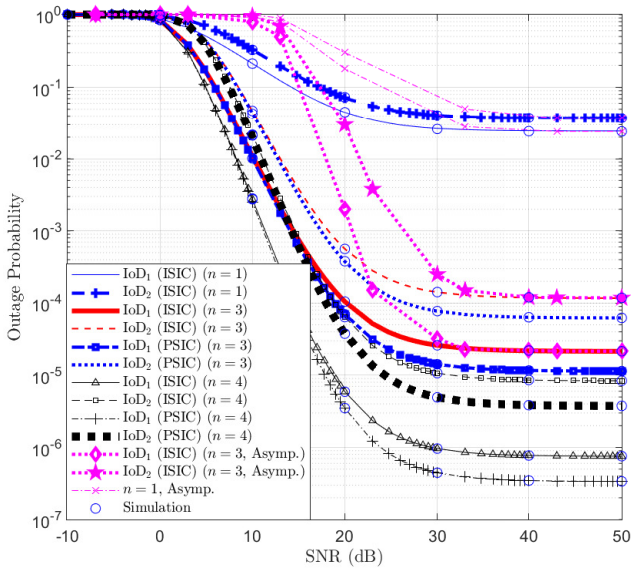

Fig. 3: OP vs SNR for $n = 1$, 3, 4, asymptotic $n = 3$ and $N = 2$ considering both PSIC-PCSI and ISIC-ICSI.

Using (62) and 63, the achievable total goodput can be computed as

$$\mathcal{G}_{Dt} = \sum\nolimits_{i=1}^{N} (\mathcal{G}_{Ri} + \mathcal{G}_{Di}). \quad (64)$$

IV. Probability of Detection Analysis

In this section, we analyze the sensing performance in terms of the false alarm and detection probabilities. Correct identification of the target is critical, when it comes to the sensing function. The existence of the target is determined by the received power. It is to be assumed that $\mathcal{H}_0$ indicates the null hypothesis, which corresponds to the absence of the target, while $\mathcal{H}_1$ indicates the presence of the target. The two hypotheses can be expressed as [11]

$$\mathcal{H}_0 : \frac{(\hat{h}_{SR} + e_{SR})y_s}{(d_{SR})^{\nu}} + \frac{(\hat{h}_{LI} + e_{LI})\sqrt{\eta P_{\text{Sen}}}\left(x_{CLI} + x_{SLI}\right)}{(d_{Li})^{\nu}} + n_R,$$

$$\mathcal{H}_1 : \frac{(\hat{h}_{SR} + e_{SR})y_s}{(d_{SR})^{\nu}} + \frac{(\hat{h}_{LI} + e_{LI})\sqrt{\eta P_{\text{Sen}}}\left(x_{CLI} + x_{SLI}\right)}{(d_{Li})^{\nu}} + \frac{(\hat{h}_{RR} + e_{RR})\sqrt{\lambda P_{\text{Sen}}}x_R}{(d_{TR})^{\nu}} + n_R. \quad (65)$$

If the received power of the AP is greater than a certain predefined sensing threshold limit under $\mathcal{H}_0$, then the AP concludes the presence of the target and the wrong consequence can happen. Otherwise, the target is sensed perfectly. These decisions can be taken from (65) based on the received power of the AP which follows a complex non-central Chi-square distribution with random variables having the degree-of-freedom (DoF) of four under $\mathcal{H}_0$ and five under $\mathcal{H}_1$. The false alarm probability can be written as [50], [51], [52]

TABLE III: Parameter settings

Parameter	Value	Parameter	Value
ν	2	d_{R1}, d_{R2}	3 m, 6 m
d_{R3}, d_{R4}	9 m, 12 m	d_{SR}	16 m
d_{TR}	60 m	d_{Li}	0.5 m
η	0.001	λ	0.1
$\sigma_R^2 = \sigma_D^2$	0.25	σ^2	0.1 μW

$$\mathscr{P}_{FA} = Q_2\left(\sqrt{\frac{2\left(\frac{|\hat{h}_{SR}|^2 P_{MD}}{d_{SR}^{\nu}} + \frac{2\eta|\hat{h}_{Li}|^2 P_{\text{Sen}}}{d_{Li}^{\nu}}\right)}{\sigma^2 + \frac{\sigma_R^2 P_{MD}}{d_{SR}^{\nu}} + \frac{2\eta\sigma_R^2 P_{\text{Sen}}}{d_{Li}^{\nu}}}}, \sqrt{\frac{2\epsilon}{\sigma^2 + \frac{\sigma_R^2 P_{MD}}{d_{SR}^{\nu}} + \frac{2\eta\sigma_R^2 P_{\text{Sen}}}{d_{Li}^{\nu}}}}\right), \quad (66)$$

where ϵ indicates the predefined sensing threshold limit. Further, $Q_{\mathscr{D}}(.,.)$ indicates generalized Marcum Q-function with order $\mathscr{D}$. On the other hand, the detection probability can be written as [11]

$$\mathscr{P}_D = Q_{\frac{5}{2}}\left(\sqrt{\frac{2\left(\frac{|\hat{h}_{SR}|^2 P_{MD}}{d_{SR}^{\nu}} + \frac{2\eta|\hat{h}_{LI}|^2 P_{\text{Sen}}}{d_{Li}^{\nu}} + \frac{\lambda P_{\text{Sen}}|h_{RR}|^2}{d_{TR}^{\nu}}\right)}{\sigma^2 + \frac{\sigma_R^2 P_{MD}}{d_{SR}^{\nu}} + \frac{2\eta\sigma_R^2 P_{\text{Sen}}}{d_{Li}^{\nu}} + \frac{\lambda\sigma_R^2 P_{\text{Sen}}}{d_{TR}^{\nu}}}}, \sqrt{\frac{2\epsilon}{\sigma^2 + \frac{\sigma_R^2 P_{MD}}{d_{SR}^{\nu}} + \frac{2\eta\sigma_R^2 P_{\text{Sen}}}{d_{Li}^{\nu}} + \frac{\lambda\sigma_R^2 P_{\text{Sen}}}{d_{TR}^{\nu}}}}\right). \quad (67)$$

Remark 5: In (66)*, the value of the sensing threshold can be obtained for a given value of $\mathscr{P}_{FA}$ and using the same sensing threshold the detection probability in* (67) *can be found. If η and λ increase, the detection probability is affected accordingly. The performance of the ability to detect a target is also subject to the degree of the CSI error, indicated by σ_R^2. For appropriate system operation, in general, the false alarm probability should be less than 10^{-3}. We also note that the non-integer order of Marcum Q-function in* (66) *can be possible to simplify further using [53].*

V. Numerical Results

The simulation parameters are given in Table III. Monte-Carlo simulation is executed to validate the analytical outputs. The power allocation factors for the common message of the two-device case are $a_p = b_c = 0.55$ and the power allocation factors for the common message of the four-device case are $a_p = 0.6$, $b_c = 0.5$. The power allocation factors for private message at the AP and at the IoDs (i.e., a_i and b_i for $i \in \{1, ..., N\}$) are presented in vector forms for $N = 4$ and 2 are correspondingly given as $\boldsymbol{\mathcal{A}} = [0.15, 0.12, 0.09, 0.04]$; $\boldsymbol{\mathcal{B}} = [0.2, 0.15, 0.09, 0.06]$ and $\boldsymbol{\mathcal{A}} = [0.25, 0.2]$; $\boldsymbol{\mathcal{B}} = [0.25, 0.2]$. The SIC imperfection vectors at the AP and IoDs for both $N = 4, 2$ are correspondingly given as $\boldsymbol{\Theta} = \boldsymbol{\Phi} = 0.35$. Υ_C^{th} and Υ_P^{th} are considered as -26 dB and -30 dB, respectively. The transmit power is considered within the range between -80 to 10 dBW which is reasonable for smart transportation, smart healthcare, and smart city applications [11].

Fig. 3 illustrates the OPs of different IoDs with respect to SNR for $N = 2$ considering both ICSI and PCSI at different values of $n = 1, 3, 4$. As shown in the figure, the simulation results are consistent with the corresponding analytical results in (16), which validate our analysis. Also, the SINRs at the AP and each device increase with the increasing transmit power from the MD and the AP. Therefore, the outage performance of IoDs improves (i.e., decreases) with higher transmit power. Furthermore, the impacts of both PSIC and ISIC on the system performance can be quantified. In the figure, as the CSI error increases, the outage performances of the IoDs also deteriorate in accordance with applying SIC. Specifically, the performance of IoD_1 is better than IoD_2 and the outage performance of IoD_1 is found to be better at $n = 4$. The asymptotic expression with $n = 3$ in (17) also shows a correlation with the simulation results at high SNR region.

Fig. 4 shows the OP with respect to the SNR for $N = 4$ considering both PSIC-PCSI and ISIC-ICSI at $n = 3$. The

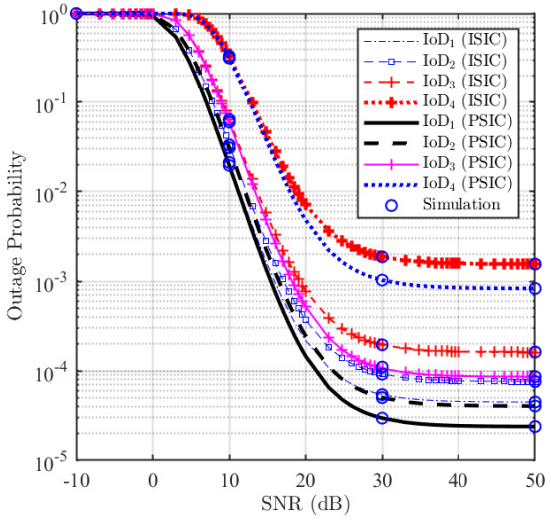

Fig. 4: OP vs SNR for $n = 3$ and $N = 4$ considering both PSIC-PCSI and ISIC-ICSI.

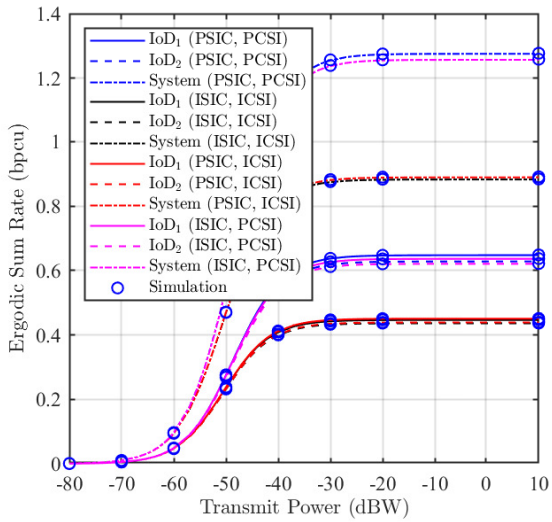

Fig. 5: Ergodic sum rate vs transmit power for $n = 3$ considering various conditions of SIC and channel state information (CSI).

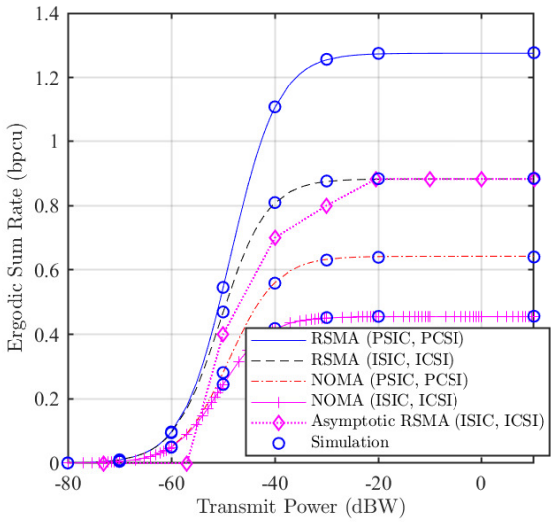

Fig. 6: Ergodic sum rate vs transmit power comparison between RSMA and NOMA for $n = 3$ considering both SIC and CSI.

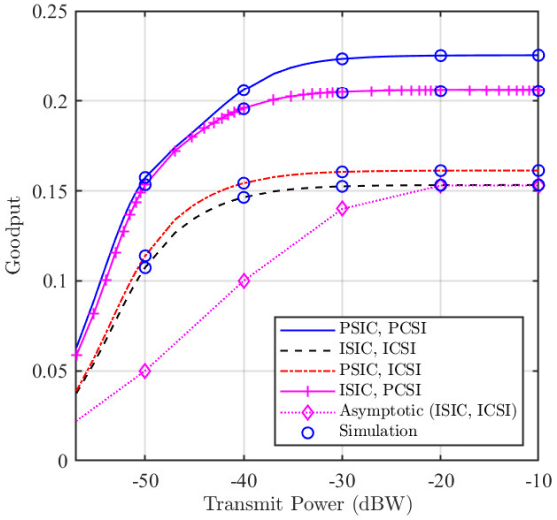

Fig. 8: Goodput vs transmit power for $n = 3$ and $N = 2$ considering both SIC and CSI.

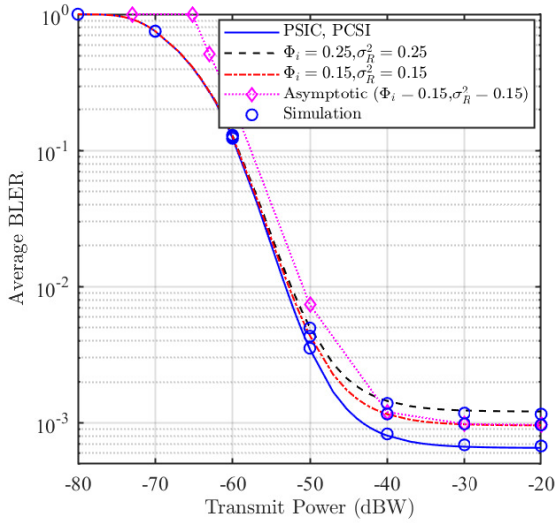

Fig. 7: BLER vs transmit power for $n = 3$ and $N = 2$ considering both SIC and CSI.

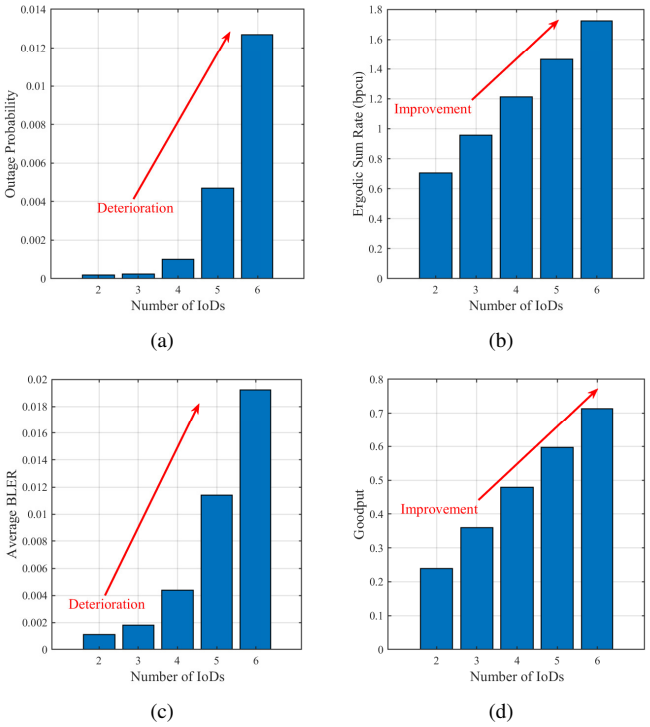

Fig. 9: Graphical plot of (a) OP, (b) Ergodic sum rate, (c) Average BLER, (d) Goodput with respect to the number of IoDs.

performance of IoD_1 is the best among all the IoDs present in the system. Since higher power is allocated to devices for $N = 2$ compared to $N = 4$, the performances of IoD_1 and IoD_2 are better for $N = 2$ compared to $N = 4$ at $n = 3$. About 52% and 35% outage performance gains are obtained for IoD_1 and IoD_2, respectively at 40 dB SNR in case of $N = 2$ compared to $N = 4$.

In Fig. 5, we investigate the ergodic sum rate with respect to transmit power for $N = 2$ considering various combinations of SIC and CSI at $n = 3$. As expected, the sum rate increases, as the transmit power increases. Moreover, the ergodic rate performance with perfect channel estimation is significantly higher compared to that with imperfect channel estimation. Further, imperfect SIC is also another key factor causing inappropriate decoding of the private message. The system performances for both ICSI-PSIC and ICSI-ISIC are considerably worse compared to PCSI-PSIC and PCSI-ISIC. We observe about 31% performance improvement for PSIC-PCSI compared to ISIC-ICSI at -20 dBW transmit power.

In Fig. 6, we compare the ergodic sum rate of NOMA and RSMA techniques for $N = 2$ considering both PSIC-PCSI and ISIC-ICSI at $n = 3$. For NOMA, a_p and b_c are set as 0, while $a_1 = b_1 = 0.9$ and $a_2 = b_2 = 0.1$. It is observed that the performances of both techniques are improved with the increasing transmit power. The sum rates of the two techniques are comparable with transmit power below -70 dB. However, with the transmit power higher than -70 dB, the ergodic rate

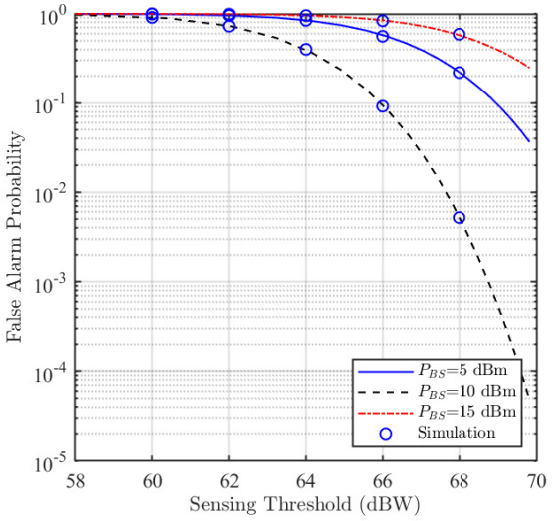

Fig. 10: False alarm probability vs ϵ for $n = 3$.

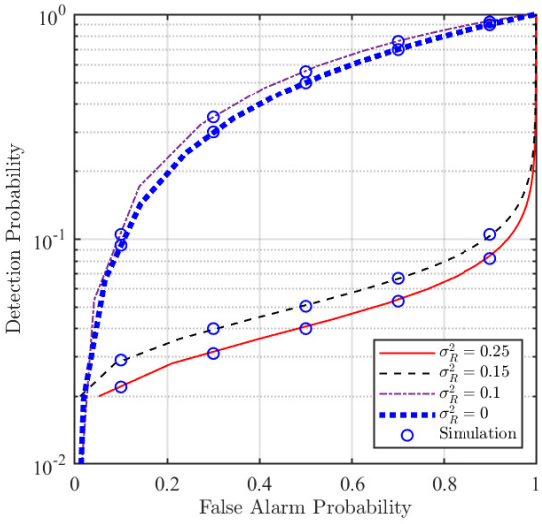

Fig. 12: Detection probability vs false alarm probability for $n = 3$.

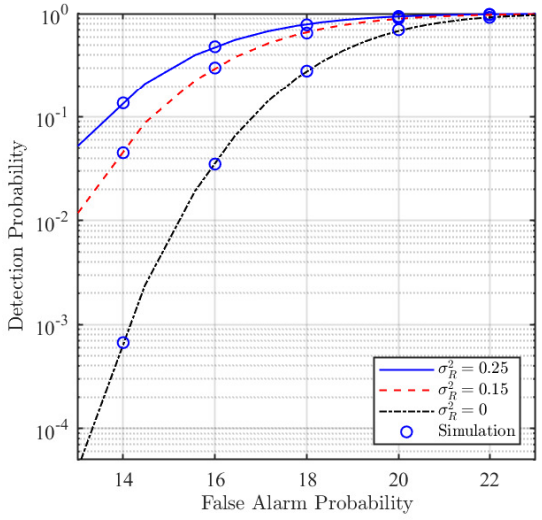

Fig. 11: False alarm probability vs transmit power for $n = 3$.

of RSMA increases much faster compared to NOMA, as the transmit power increases. We observe that the RSMA-based system is more robust compared to the NOMA-based system for both PSIC-PCSI and ISIC-ICSI. About 38% and 96% performance improvements are found for RSMA in the case of ISIC compared to NOMA with PSIC and ISIC, respectively at -20 dBW transmit power.

In Fig. 7, the average BLER for $N = 2$ is shown considering various cases of CSI and SIC conditions at $n = 3$. The BLER is also improved with the increasing transmit power. Simulation results are perfectly in line with the analytical results. Due to imperfect CSI and SIC, the system BLER performance degrades. It is also observed that the early saturation of BLER is found for more imperfection in CSI and SIC. About 42% performance improvement is found for PSIC-PCSI compared to ISIC-ICSI with ($\Phi_i = 0.25$, $\sigma_R^2 = 0.25$) at -20 dBW transmit power. The goodput performance is also shown in Fig. 8 with respect to transmit power. As the goodput is directly proportional to the complement of BLER, the goodput increases with increasing transmit power. In the figure, we observe about 53% performance improvement for PSIC-PCSI compared to ISIC-ICSI at -20 dBW transmit power.

Fig. 9a, Fig. 9b, Fig. 9c, Fig. 9d exhibit the variations of OP, ergodic sum rate, BLER and goodput with respect to number of IoDs. It is clearly seen from the figures that the reliability in terms of outage probability and BLER deteriorates, and sum rate along with goodput are improved with the increasing number of IoDs.

Fig. 10 depicts the false alarm probability with respect to ϵ for $N = 2$ and different transmit power of $P_{MD} = P_{\text{Sen}}$ at $n = 3$ and $\sigma_R^2 = 0.25$. The false alarm probability decreases with the increasing sensing threshold limit following (66). Because the SINR increases through the enhancement of P_{MD}, the false alarm probability is upgraded at higher P_{MD}. At sufficiently high ϵ, the significant variation of the false alarm probability is observed for a small change of P_{MD}. We observe almost 98% and 99% degradation in the false alarm probability at 10 dBm and 5 dBm, respectively, compared to 15 dBm transmit power. Fig. 11 shows the false alarm probability with respect to transmit power for $N = 2$ and $n = 3$ at a given ϵ as 39.5 dBW. As the channel estimation becomes more inaccurate, the false alarm probability increases at lower transmit power. The probability reaches the maximum value as 1 at 23 dBm transmit power for PCSI. About 43% and 95% improvements (decrements) of the false alarm probability are found at $\sigma_R^2 = 0.15$ and $\sigma_R^2 = 0$, respectively compared to $\sigma_R^2 = 0.25$ at 15 dBm transmit power.

Fig. 12 illustrates the detection probability with respect to the false alarm probability for $N = 2$ and $n = 3$ for given $\epsilon = 39.5$ dBW. Both probabilities of detection and false alarm deteriorate with the increase in transmit power for a given value of ϵ following (66) and (67), respectively. Therefore, the probability of detection increases with the increasing false alarm probability. Initially sluggish rate of change of the

detection probability is found and thereafter the change is faster with the variation of the false alarm probability with lower channel estimation error and reverse characteristics are to be obtained at higher channel estimation error.

VI. Conclusions

In this paper, we have investigated the RSMA-based ISAC system in IoT networks with multiple devices for higher spectral efficiency. We have derived the closed-form expressions of OP, ergodic rate, BLER, goodput over Nakagami fading channels for an arbitrary number of IoDs and the expressions of the false alarm and detection probabilities of the proposed system. For more comprehensive and realistic performance evaluation, we have considered both infinite and finite blocklength regimes under imperfect CSI and SIC, the impacts of which are captured in the derived expressions of the various performance metrics. The analytical results have been verified through Monte-Carlo simulations. Further, we have observed that system performances in terms of the OP, ergodic sum rate, BLER, and goodput are considerably degraded by ICSI and ISIC. In addition, the proposed RSMA-based ISAC provides higher ergodic sum rates compared to NOMA both in the presence and absence of the CSI and SIC errors. For the sensing capability, we have shown how the probabilities of detection and false alarm change under varying sensing threshold and SNR and, in particular, the significant performance loss caused by ICSI. Our analytical and simulation results can provide insights into the design of the RSMA-based ISAC system under practical impairments.

It is noted that the ISAC system considered in this work can be used in various applications such as autonomous driving, vehicle-to-everything (V2X), urban air mobility (UAM), smart city/home, and healthcare [54]. Further, the third generation partnership project (3GPP) in [55] defines practical use cases of the ISAC technology such as intruder detection, UAV flight trajectory tracing, positioning in factories, public safety search and rescue, rainfall monitoring, healthcare, and gesture recognition. In addition, future extensions of this work may include multi-group multicast channels, multi-cell multi-cast multiple targets detection, etc. The issue of secure multicast in ISAC-based networks is also an interesting topic, which can improve the robustness of the system.

Acknowledgement

The work of T. Q. Duong was supported in part by the Canada Excellence Research Chair (CERC) Program CERC-2022-00109.

References

[1] Y. Cui, F. Liu, X. Jing, and J. Mu, "Integrating sensing and communications for ubiquitous IoT: applications, trends, and challenges," *IEEE Netw.*, vol. 35, no. 5, pp. 158 – 167, 2021.

[2] F. Wang and H. Li, "Joint power allocation for multicarrier Radar and communication coexistence," in *Proc. IEEE RADAR Conference, Washington, DC, USA*, 2020, pp. 141 – 145.

[3] T. Wild, V. Braun, and H. Viswanathan, "Joint design of communication and sensing for beyond 5G and 6G systems," *IEEE Access*, vol. 9, pp. 30 845 – 30 857, 2021.

[4] F. Liu, C. Masouros, A. Li, H. Sun, and L. Hanzo, "MU-MIMO communications with MIMO Radar: from co-existence to joint transmission," *IEEE Trans. Wireless Commun.*, vol. 17, no. 4, pp. 2755–2770, 2018.

[5] Z. Cui, J. Hu, J. Cheng, and G. Li, "Multi-domain NOMA for ISAC: utilizing the DOF in the delay-doppler domain," *IEEE Commun. Lett.*, vol. 27, no. 2, pp. 726 – 730, 2023.

[6] F. Liu, Y. Cui, C. Masouros, J. Xu, T. X. Han, Y. C. Eldar, and S. Buzzi, "Integrated sensing and communications: toward dual-functional wireless networks for 6G and beyond," *IEEE J. Sel. Areas Commun.*, vol. 40, no. 6, pp. 1728–1767, 2022.

[7] C. Dou, N. Huang, Y. Wu, L. Qian, and T. Q. S. Quek, "Channel sharing aided integrated sensing and communication: An energy-efficient sensing scheduling approach," *IEEE Trans. Wireless Commun.*, 2023.

[8] J. Hu, Q. Lin, S. Yan, X. Zhou, Y. Chen, and F. Shu, "Covert transmission via integrated sensing and communication systems," *IEEE Trans. Veh. Technol.*, pp. 1–6, 2023.

[9] Z. Yang, D. Li, N. Zhao, Z. Wu, Y. Li, and D. Niyato, "Secure precoding optimization for NOMA-aided integrated sensing and communication," *IEEE Trans. Commun.*, vol. 70, no. 12, pp. 8370–8382, 2022.

[10] C. Xu, B. Clerckx, S. Chen, Y. Mao, and J. Zhang, "Rate-splitting multiple access for multi-antenna joint radar and communications," *IEEE J. Sel. Topics Signal Process*, vol. 15, no. 6, pp. 1332–1347, 2021.

[11] M. Liu, M. Yang, H. Li, K. Zeng, Z. Zhang, A. Nallanathan, G. Wang, and L. Hanzo, "Performance analysis and power allocation for cooperative ISAC networks," *IEEE Internet Things J.*, vol. 10, no. 7, pp. 6336–6351, 2023.

[12] C. Dou, N. Huang, Y. Wu, L. Qian, and T. Q. Quek, "Sensing-efficient NOMA-aided integrated sensing and communication: a joint sensing scheduling and beamforming optimization," *IEEE Trans. Vehicular Tech.*, pp. 1–14, 2023.

[13] L. Yin, Y. Mao, O. Dizdar, and B. Clerckx, "Rate-splitting multiple access for 6G—part ii: interplay with integrated sensing and communications," *IEEE Commun. Lett.*, vol. 26, no. 10, pp. 2237 – 2241, 2022.

[14] C. Zhang, W. Yi, Y. Liu, and L. Hanzo, "Semi-integrated-sensing-and-communication (semi-ISAC): from OMA to NOMA," *IEEE Trans. Commun.*, vol. 71, no. 4, pp. 1878 – 1893, 2023.

[15] J. A. Mahal, A. Khawar, A. Abdelhadi, and T. C. Clancy, "Spectral coexistence of MIMO radar and MIMO cellular system," *IEEE Trans. Aerosp. Electron. Syst.*, vol. 53, no. 2, pp. 655–668, 2017.

[16] Q. Zhang, H. Sun, Z. Wei, and Z. Feng, "Sensing and communication integrated system for autonomous driving vehicles," in *Proc. IEEE INFOCOM Workshops, Toronto, ON, Canada*, 2020, pp. 1278–1279.

[17] X. Mu, Z. Wang, and Y. Liu, "NOMA for integrating sensing and communications towards 6G: a multiple access perspective," *IEEE Wireless Commun.*, pp. 1–8, 2023.

[18] C. Ouyang, Y. Liu, and H. Yang, "Revealing the impact of SIC in NOMA-ISAC," *IEEE Wireless Commun. Lett.*, vol. 12, no. 10, pp. 1707–1711, 2023.

[19] M. Liu, M. Yang, and A. Nallanathan, "On the performance of uplink and downlink integrated sensing and communication systems," in *Proc. IEEE Globecom Workshops, Rio de Janeiro, Brazil*, 2022, pp. 1236–1241.

[20] D. Tse and P. Viswanath, *Fundamentals of wireless communication*. Cambridge university press, 2005.

[21] Z. Wang, Y. Liu, X. Mu, and Z. Ding, "NOMA inspired interference cancellation for integrated sensing and communication," in *Proc. IEEE International Conference on Communications, Seoul, Korea*, 2022, pp. 3154–3159.

[22] E. Memisoglu, H. Türkmen, B. A. Ozbakis, and H. Arslan, "CSI-based NOMA for integrated sensing and communication," *IEEE Wireless Commun. Lett.*, vol. 12, no. 6, pp. 1086–1090, 2023.

[23] L. Bariah, S. Muhaidat, P. C. Sofotasios, F. E. Bouanani, O. A. Dobre, and W. Hamouda, "Large intelligent surface-assisted nonorthogonal multiple access for 6G networks: Performance analysis," *IEEE Internet Things J.*, vol. 8, no. 7, pp. 5129–5140, 2021.

[24] X. Li, J. Li, Y. Liu, Z. Ding, and A. Nallanathan, "Residual transceiver hardware impairments on cooperative NOMA networks," *IEEE Trans. Wireless Commun.*, vol. 19, no. 1, pp. 680–695, 2020.

[25] L. Zhang, J. Liu, M. Xiao, G. Wu, Y.-C. Liang, and S. Li, "Performance analysis and optimization in downlink NOMA systems with cooperative full-duplex relaying," *IEEE J. Sel. Areas Commun.*, vol. 35, no. 10, pp. 2398–2412, 2017.

[26] Y. Mao, B. Clerckx, and V. O. Li, "Rate-splitting multiple access for downlink communication systems: bridging, generalizing, and outperforming SDMA and NOMA," *EURASIP J. Wireless Commun. Netw.*, vol. 2018, pp. 1–54, 2018.

[27] X. Lyu, S. Aditya, J. Kim, and B. Clerckx, "Rate-splitting multiple access: The first prototype and experimental validation of its superiority over SDMA and NOMA," *IEEE Trans. Wireless Commun.*, 2024.

[28] B. Clerckx, Y. Mao, R. Schober, and H. V. Poor, "Rate-splitting unifying SDMA, OMA, NOMA, and multicasting in MISO broadcast channel: a simple two-user rate analysis," *IEEE Wireless Commun. Lett.*, vol. 9, no. 3, pp. 349–353, 2020.

[29] W. Jaafar, S. Naser, S. Muhaidat, P. C. Sofotasios, and H. Yanikomeroglu, "Multiple access in aerial networks: from orthogonal and non-orthogonal to rate-splitting," *IEEE Open J. Veh. Technol.*, vol. 1, pp. 372–392, 2020.

[30] Y. Mao, O. Dizdar, B. Clerckx, R. Schober, P. Popovski, and H. V. Poor, "Rate-splitting multiple access: fundamentals, survey, and future research trends," *IEEE Commun. Surveys Tuts.*, vol. 24, no. 4, pp. 2073–2126, 2022.

[31] S. K. Singh, K. Agrawal, K. Singh, and C.-P. Li, "Ergodic capacity and placement optimization for RSMA-enabled UAV-assisted communication," *IEEE Systems J.*, vol. 17, no. 2, pp. 2586–2589, 2023.

[32] S. K. Singh, K. Agrawal, K. Singh, B. Clerckx, and C.-P. Li, "RSMA for hybrid RIS-UAV-aided full-duplex communications with finite block-length codes under imperfect SIC," *IEEE Trans. Wireless Commun.*, 2023.

[33] L. Yin and B. Clerckx, "Rate-splitting multiple access for dual-functional radar-communication satellite systems," in *Proc. IEEE Wireless Communications and Networking Conference, Austin, TX, USA*, 2022, pp. 1–6.

[34] L. Yin, Z. Liu, M. R. Bhavani Shankar, M. Alaee-Kerahroodi, and B. Clerckx, "Integrated sensing and communications enabled low earth orbit satellite systems," *IEEE Netw.*, 2024.

[35] T. Riihonen, S. Werner, and R. Wichman, "Mitigation of loopback self-interference in full-duplex MIMO relays," *IEEE Trans. Signal Process.*, vol. 59, no. 12, pp. 5983–5993, 2011.

[36] A. R. Chiriyath, B. Paul, and D. W. Bliss, "Simultaneous radar detection and communications performance with clutter mitigation," in *Proc. IEEE Radar Conference, Seattle, WA, USA*, 2017, pp. 279–284.

[37] Z. Xiao and Y. Zeng, "Waveform design and performance analysis for full-duplex integrated sensing and communication," *IEEE J. Sel. Areas Commun.*, vol. 40, no. 6, pp. 1823–1837, 2022.

[38] B. Clerckx, H. Joudeh, C. Hao, M. Dai, and B. Rassouli, "Rate splitting for MIMO wireless networks: a promising PHY-layer strategy for LTE evolution," *IEEE Commun. Mag.*, vol. 54, no. 5, pp. 98–105, 2016.

[39] H. Joudeh and B. Clerckx, "Sum-rate maximization for linearly precoded downlink multiuser MISO systems with partial CSIT: a rate-splitting approach," *EEE Trans. Commun.*, vol. 64, no. 11, pp. 4847–4861, 2016.

[40] G. L. Stuber, *Principles of mobile communication*, 2nd ed. Kluwer Academic Publisher, 2002.

[41] M. Can and I. Altunbas, "Outage probability analysis of rate splitting multiple access-based hybrid satellite-terrestrial relay network with relay selection," *IEEE Trans. on Aerosp. and Electron. Syst.*, 2023.

[42] I. S. Gradshteyn and I. M. Ryzhik, *Table of integrals, series, and products*. Academic press, 2014.

[43] F. W. J. Olver, "Uniform asymptotic expansions for Weber parabolic cylinder functions of large orders," *J. Res. Nat. Bur. Standards Sect. B*, vol. 63, no. 2, pp. 131–169, 1959.

[44] A. A. Nasir, X. Zhou, S. Durrani, and R. A. Kennedy, "Throughput and ergodic capacity of wireless energy harvesting based DF relaying network," in *Proc. IEEE International Conference on Communications, Sydney, NSW*, 2014, pp. 4066–4071.

[45] N. H. Tu and K. Lee, "Performance analysis and optimization of multihop MIMO relay networks in short-packet communications," *IEEE Trans. Wireless Commun.*, vol. 21, no. 6, pp. 4549–4562, 2022.

[46] B. Makki, T. Svensson, and M. Zorzi, "Finite block-length analysis of the incremental redundancy HARQ," *IEEE Wireless Commun. Lett.*, vol. 3, no. 5, pp. 529–532, 2014.

[47] S. K. Singh, K. Agrawal, K. Singh, Y.-M. Chen, and C.-P. Li, "Performance analysis and optimization of RSMA enabled UAV-aided IBL and FBL communication with imperfect SIC and CSI," *IEEE Trans. Wireless Commun.*, vol. 22, no. 6, pp. 3714–3732, 2023.

[48] C. D. Ho, T.-V. Nguyen, T. Huynh-The, T.-T. Nguyen, D. B. da Costa, and B. An, "Short-packet communications in wireless-powered cognitive IoT networks: performance analysis and deep learning evaluation," *IEEE Trans. Veh. Technol.*, vol. 70, no. 3, pp. 2894–2899, 2021.

[49] P. Raut, P. K. Sharma, T. A. Tsiftsis, and Y. Zou, "Power-time splitting-based non-linear energy harvesting in FD short-packet communications," *IEEE Trans. Veh. Technol.*, vol. 69, no. 8, pp. 9146–9151, 2020.

[50] Z. Zhang, B. Chen, and M. Yang, "Moving target detection based on time reversal in a multipath environment," *IEEE Trans. Aerosp. Electron. Syst.*, vol. 57, no. 5, pp. 3221–3236, 2021.

[51] A. R. Chiriyath and D. W. Bliss, "Effect of clutter on joint radar-communications system performance inner bounds," in *Proc. IEEE Asilomar Conference on Signals, Systems and Computers, Pacific Grove, CA*, 2015, pp. 1379–1383.

[52] D. W. Bliss and S. Govindasamy, *Adaptive wireless communications*. Cambridge University Press, 2013.

[53] A. Annamalai, C. Tellambura, and J. Matyjas, "A new twist on the generalized Marcum Q-function QM(a, b) with fractional-order M and its applications," in *Proc. IEEE Consumer Communications and Networking Conference, Las Vegas, NV, USA*, 2009, pp. 1–5.

[54] Z. Wei, F. Liu, C. Masouros, N. Su, and A. P. Petropulu, "Toward multi-functional 6G wireless networks: Integrating sensing, communication, and security," *IEEE Commun. Mag.*, vol. 60, no. 4, pp. 65–71, 2022.

[55] 3GPP, *Feasibility Study on Integrated Sensing and Communication*, V19.2.0, TR 22.837, Dec. 2023.

Sutanu Ghosh (Member, IEEE) received the M.Tech. degree from Jadavpur University, Kolkata, India, in 2009, and the Ph.D. degree from the Indian Institute of Engineering Science and Technology Shibpur, Howrah, India, in 2021. He is currently an Associate Professor with the Department of Electronics and Communication Engineering, Institute of Engineering and Management, Kolkata, and also working as a Visiting Research Scholar with the Computer, Electrical and Mathematical Science and Engineering Division, King Abdullah University of Science and Technology, Thuwal, Saudi Arabia. His research interests include radio-frequency energy harvesting, visible light communication, Internet of Things, and cognitive radio networks.

Keshav Singh (Member, IEEE) received the M.Sc. degree in information and telecommunications technologies from Athens Information Technology, Greece, in 2009, and the Ph.D. degree in communication engineering from the National Central University, Taiwan, in 2015. He currently works at the Institute of Communications Engineering, National Sun Yat-sen University (NSYSU), Taiwan, as an Associate Professor. Prior to this, he held the position of research associate at the Institute of Digital Communications, The University of Edinburgh, U.K., from 2016 to 2019. From 2019 to 2020, he was associated with the University College Dublin, Ireland, as a Research Fellow. He leads research in the areas of green communications, resource allocation, full-duplex radio, ultra-reliable low-latency communication, non-orthogonal multiple access, wireless edge caching, machine learning for communications, and large intelligent surface-assisted communications.

Haejoon Jung (Senior Member, IEEE) received the B.S. degree (Hons.) from Yonsei University, South Korea, in 2008, and the M.S. and Ph.D. degrees from the Georgia Institute of Technology (Georgia Tech), Atlanta, GA, USA, in 2010 and 2014, respectively, all in electrical engineering. From 2014 to 2016, he was a Wireless Systems Engineer at Apple, Cupertino, CA, USA. From 2016 to 2021, he was with Incheon National University, Incheon, South Korea. Since September 2021, he has been with the Department of Electronic Engineering, Kyung Hee University, as an Associate Professor. His research interests include communication theory, wireless communications, wireless power transfer, and statistical signal processing. He was a recipient of the Haedong Young Scholar Award from the Korean Institute of Communications and Information Sciences (KICS) in 2022. He serves as an Editor for IEEE Transactions on Vehicular Technology, IEEE Transactions on Aerospace and Electronic Systems, IEEE Communications Letters, IEEE Wireless Communications Letters, and ICT Express.

Chih-Peng Li (Fellow, IEEE) was born in Taiwan, R.O.C., on September 30, 1967. He received the B.S. degree from National Tsing-Hua University in 1989, the M.S. degree in electrical engineering from Syracuse University, Syracuse, NY, in 1993, and the Ph.D. degree in electrical engineering from Cornell University, Ithaca, NY, in 1997.,From January 1996 to December 1997, he was a Teaching Assistant at Cornell University. He joined the Wireless Technology Laboratory, Lucent Technologies, Whippany, NJ, in January 1998. He was a member of Technical Staff, Bell Lab, Lucent Technology, Whippany, NJ. His research interests include mobile radio, computer networks, and digital communications. He is currently with the Institute of Communication Engineering, National Sun Yat-Sen University, Kaohsiung, Taiwan, R.O.C.

Trung Q. Duong (Fellow, IEEE) is a Canada Excellence Research Chair (CERC) and a Full Professor at Memorial University, Canada. He is also the adjunct Chair Professor in Telecommunications at Queen's University Belfast, UK and a Research Chair of Royal Academy of Engineering, UK. He was a Distinguished Advisory Professor at Inje University, South Korea (2017-2019), an Adjunct Professor and the Director of Institute for AI and Big Data at Duy Tan University, Vietnam (2012-present), and a Visiting Professor (under Eminent Scholar program) at Kyung Hee University, South Korea (2023-2025). His current research interests include quantum communications, wireless communications, quantum machine learning, and quantum optimisation.

Dr. Duong has served as an Editor/Guest Editor for the IEEE TRANSACTIONS ON WIRELESS COMMUNICATIONS, IEEE TRANSACTIONS ON COMMUNICATIONS, IEEE TRANSACTIONS ON VEHICULAR TECHNOLOGY, IEEE COMMUNICATIONS LETTERS, IEEE WIRELESS COMMUNICATIONS LETTERS, IEEE WIRELESS COMMUNICATIONS, IEEE COMMUNICATIONS MAGAZINES, and IEEE JOURNAL ON SELECTED AREAS IN COMMUNICATIONS. He received the Best Paper Award at the IEEE VTC-Spring 2013, IEEE ICC 2014, IEEE GLOBECOM 2016, 2019, 2022, IEEE DSP 2017, IWCMC 2019, 2023, and IEEE CAMAD 2023. He has received the two prestigious awards from the Royal Academy of Engineering (RAEng): RAEng Research Chair (2021-2025) and the RAEng Research Fellow (2015-2020). He is the recipient of the prestigious Newton Prize 2017.